Accepted Manuscript

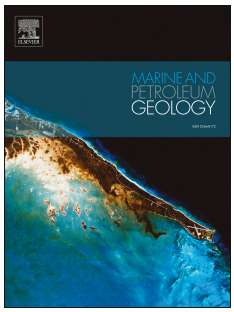

Diagenetic characteristics, evolution, controlling factors of diagenetic system and their impacts on reservoir quality in tight deltaic sandstones: Typical example from the Xujiahe Formation in Western Sichuan Foreland Basin, SW China

Long Luo, Wanbin Meng, Jon Gluyas, Xianfeng Tan, Xianzhi Gao, Mingshi Feng, Xiangye Kong, Hengbo Shao

PII: S0264-8172(19)30074-1

DOI: https://doi.org/10.1016/j.marpetgeo.2019.02.012

Reference: JMPG 3725

To appear in: *Marine and Petroleum Geology*

Received Date: 20 August 2018

Revised Date: 29 December 2018

Accepted Date: 11 February 2019

Please cite this article as: Luo, L., Meng, W., Gluyas, J., Tan, X., Gao, X., Feng, M., Kong, X., Shao, H., Diagenetic characteristics, evolution, controlling factors of diagenetic system and their impacts on reservoir quality in tight deltaic sandstones: Typical example from the Xujiahe Formation in Western Sichuan Foreland Basin, SW China, *Marine and Petroleum Geology* (2019), doi: https://doi.org/10.1016/j.marpetgeo.2019.02.012.

Diagenetic characteristics, evolution, controlling factors of diagenetic system and their impacts on reservoir quality in tight deltaic sandstones: Typical example from the Xujiahe Formation in Western Sichuan Foreland Basin, SW China

Long Luo[a,b,c]*, Wanbin Meng[d]**, Jon Gluyas[c], Xianfeng Tan[e], Xianzhi Gao[a,b],, Mingshi Feng[d], Xiangye Kong[f], Hengbo Shao[a,b]

[a] State Key Laboratory of Petroleum Resources and Prospecting, China University of Petroleum, Beijing, Beijing102249, China

[b] College of Geosciences, China University of Petroleum, Beijing 102249, China

[c] Department of Earth Sciences, Durham University, Durham, DH1 3LE, UK

[d] State Key Laboratory of Oil-Gas Reservoir Geology& Exploitation, Chengdu University of Technology, Chengdu 610059, China

[e] College of petroleum and gas Engineering, Chongqing University of Science and Technology, Chongqing 401331, China

[f] Unconventional Natural Gas Institute, China University of Petroleum, Beijing, 102249, China; State Key Laboratory of Petroleum Resources and Prospecting (China University of Petroleum, Beijing) , Beijing 102249, China.

*Corresponding author: College of Geosciences, China University of Petroleum (Beijing), Beijing 102249, China.

**Corresponding author:

State Key Laboratory of Oil-Gas Reservoir Geology& Exploitation, Chengdu University of Technology, Chengdu 610059, China

E-mail address: longluo988@163.com (L. Luo). mwb@cdut.edu.cn (W. Meng).

Abstract

Deeply buried (3000-5000 m), deltaic sandstones of the Upper Triassic Xujiahe Formation are important tight gas reservoirs in the Sichuan Foreland Basin, China. The diagenesis of these tight sandstones was examined using a variety of petrographic and geochemical techniques, including thin section description, X-ray diffraction (XRD), whole-rock chemical analysis, scanning electron microscopy (SEM), Cathodoluminescence (CL) imaging, electron probe analysis, fluid inclusions and

isotopic analysis. These integrated petrographic and geochemical techniques were used to determine the diagenetic history of the sandstones and its impact on the reservoir quality.

The tight deltaic sandstones of the T_3x^2 and T_3x^4 (second and fourth members of Xujiahe Formation) have undergone a significant and complicated series of diagenetic alterations and changes in geochemical composition. Strong mechanical and chemical compaction together with carbonate cementation destroyed almost all the primary pores and the secondary dissolution pores now dominate the pore space. The T_3x^4 sandstones experienced a more open diagenetic system at near-surface and eodiagensis resulted in higher porosity than seen in the T_3x^2 sandstones. Both the T_3x^2 and T_3x^4 sandstones experienced closed-system diagenesis during middle-late mesodiagenesis. The early diagenetic dissolution, which mainly occurred in the open geochemical system, produced secondary pores and provided kaolinite and some K^+ needed for the subsequent illitization of kaolinite and K-feldspar. The late dissolution of K-feldspar and illitization of K-feldspar in T_3x^4 sandstones and T_3x^2 sandstones during the mesodiagenesis, produced some effective secondary pores in the closed geochemical system or in the focused fluid flow zone along fractures. The diagenetic characteristics, size and evolution of (open vs closed) diagenetic system, which were constrained by the depositional environment, deep burial depth and tectonic activity, can be used to predict the reservoir quality ahead of drilling.

Keywords:

Tight deltaic sandstone; Diagenetic system; Mass transfer; Deep burial; Reservoir quality; Xujiahe Formation; Western Sichuan Foreland basin

1. Introduction

The concept of a diagenetic system was first proposed in the 1970s and 1980s,

when sandstone diagenesis and the diagenetic alteration of adjacent mudstones were discussed together as systems (Boles and Franks, 1979; Surdam et al., 1989; Gluyas and Coleman,1992). Only a few articles discuss diagenesis in terms of open and closed system in terms of element mobility during the processes of mineral precipitation and dissolution (Gluyas and Coleman, 1992; Gluyas et al, 2000; Day-Stirrat et al., 2010; Bjørlykke, 2011; Day-Stirrat et al., 2011; Bjørlykke and Jahren, 2012; Yuan et al., 2015a; Yuan et al., 2015b; Yuan et al., 2017a; Yuan et al., 2017b). For a closed diagenetic system, the bulk chemical composition of the sediment does not change significantly during burial diagenesis, and there is a mass balance between mineral dissolution and precipitation (Bjørlykke and Jahren, 2012). On the contrary, the open diagenesis system is characterized by the significant enrichment or reduction in bulk chemical composition for some elements owing to the fluid flow and transport of solutes into or out of the system (Bjørlykke and Jahren, 2012; Bjørlykke, 2014; Yuan et al.,2015b). There is evidence of open system diagenesis (Gluyas and Leonard,1995; Day-Stirrat et al., 2010; Day-Stirrat et al., 2011; Bjørlykke and Jahren, 2012; Yuan et al., 2015b) and of closed system diagenesis especially during deep burial because of limited flow rate and concentration gradients of pore-water flow (Gluyas et al, 2000; Clark, 2014).

In a closed diagenetic (geochemical) system, predictions about rock properties or reservoir quality can be achieved with respect to rock properties as a function of burial history and diagenetic reactions and sediment composition (Gluyas, 1997; Gluyas and Witton, 1997) and written as balanced chemical equations (Bjørlykke, 2010; Bjørlykke and Jahren, 2012). However, the reservoir quality is not easy to forecast in the open diagenesis system, because the diagenetic characteristics (type, sequence and origin) and controlling factors are complex and changeable and the

processes of mass and transport required for an open system are rarely well understood (Bjørlykke and Jahren, 2012; Bjørlykke .2014).

The deltaic sandstone of the Upper Triassic Xujiahe Formation is an important tight gas reservoir in the Western Sichuan Foreland Basin of China (Tang et al., 2009). The deeply buried, tight deltaic sandstone of the Upper Triassic Xujiahe Formation have generally undergone complicated diagenetic alterations which have reduced the reservoir quality (Meng et al.,2013; Liu et al.,2014a, b; Luo et al.,2015). The Xujiahe Formation may have experienced an open diagenetic system during burial process because it experienced several hydrogeological and tectonic (fracture formation) events within its geological history (Zheng et al., 2003; Shen et al., 2010).

The aim of this study was to understand the diagenetic evolution of tight gas sandstones belonging to the Triassic, Xujiahe Formation, Sichuan Foreland Basin, SW China (Fig.1) in order that in unexplored regions of the basin the reservoir quality can be forecast ahead of drilling. Both porosity and permeability are generally low in the Xujiahe Formation but there are intervals with higher permeability (>0.1mD) that dominate gas flow and as such it is necessary to understand how the diagenetic system evolved in order to forecast the occurrence of such zones.

2. Geological setting

2.1 Basin evolution

The Sichuan Basin, in southwestern China, is a diamond-shaped foreland basin surrounded by thrust belts on all sides (Xu et al., 2015) (Fig. 1). This superimposed basin has undergone two tectonic and corresponding depositional cycles: the Sinian-Middle Triassic tectonic evolution of a passive continental margin and the Late Triassic-Eocene evolution of a foreland basin (Ni et al., 2014, Lai et al., 2015). From the Early to Middle Triassic, the cratonic margins of the Sichuan Basin were raised as

a result of the compression of the Tethys and Pacific Plates (Lai et al., 2015). In the Late Triassic, the Sichuan Basin evolved into a foreland basin with the uplift of the Longmen Mountain at its western margin (Tao et al., 2014); therefore, the Western Sichuan foreland basin, located in the Western Sichuan Basin, developed after the Late Triassic (Fig. 1, Wang, 2012).

The Xinchang structural belt, located in the central region of the Western Sichuan Foreland Basin (depression, Fig. 1), is a large multistage uplift that began in the late Indo-Chinese epoch（Late Triassic）, developed during the Yanshanian Period (Triassic - Cretaceous), and eventually finished forming during the Himalayan (Ye et al., 2009).

2.2. Stratigraphy and depositional facies

The stratigraphic column of the Western Sichuan depression shows that the Upper Triassic Xujiahe Formation (roughly equivalent to the Upper Triassic Norian stage) generally comprises its second member (T_3x^2), third member (T_3x^3), fourth member (T_3x^4) and fifth member (T_3x^5) (Fig. 2) (Zheng et al.,2003). The first member of the Xujiahe Formation (T_3x^1), which represents the critical source rock, is generally divided into the Xiaotangzi and Maantang intervals, because it was deposited in shallow sea or marine prodelta environment that was significantly different from the continental or transitional environments of other members of the Xujiahe Formation, (Lin, 2005). The second (T_3x^2) (burial depth >4600m;thickness 560-660m)and fourth (T_3x^4) (burial depth 3000-4000m;thickness 536-610m)members of the Xujiahe Formation mainly consist of deltaic sandstones, which are the major sandstone reservoirs of the study area (Fig. 2). The second member of the Xujiahe Formation (T_3x^2) was mainly deposited in a marine delta front belonging to a marine-to-continent transitional environment, which mainly consists of

distributary channel and mouth bar sandstones (Lin, 2005; Shi,2010). However, the fourth member (T_3x^4) was deposited in the lacustrine braided-river delta front of continent sedimentary environment, in which, underwater distributary channel and mouth bar are the dominant microfacies (Lin, 2005; Shi,2010). The third (T_3x^3) and fifth(T_3x^5) members of the Xujiahe Formation were deposited in a lacustrine braid-river delta plain that is dominated by swamp microfacies and branch channel, so both the T_3x^3 and T_3x^5 are important source rocks and coal-bearing strata (Lin, 2005; Shi, 2010).

2.3 Diagenetic geochemical system

Fractures are important fluid-flow conduits and a significant part of the reservoir pore volume in the Xujiahe Formation (Zhang, 2005; Zeng, 2010; Luo, 2015). The fractures were controlled by the tectonic activity and are critical to large-scale convection of fluid in the reservoir because of their high permeability (Zhang, 2005; Zeng, 2010). The fractures in the T_3x^2 member started to form at the end of the Triassic (the Late Indosinian), and continued forming during the Yanshanian and Himalayan (Zhang, 2005). The initial stage of fracturing within the T_3x^4 member was at the end of the Middle Yanshanian, and subsequent stages were late Yanshanian and Himalayan (Zhang, 2005). Consequently, the abundant fractures in the Xujiahe Formation provide crucial migration pathways for fluid flow and transport of solutes .

Cross-formational migration of fluids in the Upper Triassic drove homogenisation of formation water geochemistry in the T_3x^2 and T_3x^4 members (Zheng et al., 2003; Shen et al 2010). The original formation water within the T_3x^2 and T_3x^4 were almost completely replaced by the formation water from the coal-bearing strata (e.g. T_3x^3 and T_3x^5) and the underlying marine mudstone of the T_3x^1 member (Shen et al., 2010). These previous studies indicate the possible

existence of an open geochemical system in the Xujiahe Formation (T_3x^2 and T_3x^4) during burial process from near-surface to deep burial (Liu, 2010; Shen et al., 2010).

3. Materials and methods

Rock composition data for 7068 thin sections samples (4254 fromT_3x^2 and 2814 from T_3x^4 of related 32 wells) and 6550 porosity and permeability data pairs (2760 from T_3x^2 core sandstone samples and 3790 from T_3x^4 sandstone) were provided by the Research Institute of Petroleum Exploration & Development of the Southwest Oil-Gas Branch Company, Sinopec.

Based on the objectives of this study, 250 sandstone samples (sampling interval ~ 0.5 m) were collected from the T_3x^2 and T_3x^4 members in drill cores of 32 wells (Fig. 1C), in which 220 thin sections (18 key wells with hydrocarbon shows) were impregnated with blue epoxy resin and prepared for mineralogical and diagenetic studies (Fig. 1C). Thin sections were partly stained with Alizarin Red S and K-ferricyanide for carbonate mineral identification. Point counting (300 points per thin section) analysis , in which the composition of 300 points per thin-section will be identified and counted, was performed on 40 thin sections collected from 40 drill cores of T_3x^2 and T_3x^4 members in 10 key wells to quantify rock composition and confirm the previously collected rock composition data and diagenetic relationships (Van der Plas and Tobi, 1965;Yuan et al.,2015a,b; Hansen et al.,2017). Cements in the 40 thin sections were identified and photographed under the microscope with digital camera and sketched on a computer using the CorelDRAW software, and the corresponding area of each cement in the photomicrographs was calculated using Image-Pro Plus software. Finally, the bulk percentage of each cement was calculated by determining the average value of area rates in 10 photomicrographs from the same thin section.

150 core representative samples (from the main reservoir sandstone of key wells with hydrocarbon shows) were coated with gold and examined under a Quanta250 FEG scanning electron microscope (SEM) equipped with an Oxford INCAx-max20 energy dispersive spectroscope (EDS). Cathodoluminescence (CL) analyses of 20 typical core samples, in which carbonate cement was relatively well developed (> 2%), were completed using an Olympus microscope equipped with a CL8200-MKS CL instrument.

Eighty-five carbonate grains, including carbonate cements and rock fragments, were analysed for their C and O isotopic compositions in situ using the laser microsampling technique with a MAT252 Gas Isotope Ratio Mass Spectrometer at the Research Institute of Exploration and Development of the Southwest Oil-Gas field Company, Petrochina. The selected carbonate minerals produced CO_2 gas by heating the specified micro-zone of thin-section inside the vacuum sample box with high-energy laser beam. Then the CO_2 gas was purified by vacuum and sent into mass spectrometer for measurement of carbon and oxygen isotope. The precision was ±0.08‰ for oxygen and ±0.06‰ for carbon.

Twenty core samples with quartz cement (more than 2%) were prepared as thick doubly polished sections of 100 μm thickness for microthermometric measuement of fluid inclusions using a petrographic microscope equipped with a Linkam. The THMSG 600 heating and cooling stage enables the temperatures of phase transitions ranging from -180 to 600°C. Inclusions within quartz cement were photographed with digital camera for the purpose of fast mapping of inclusion locations. The homogenization temperature (Th) were determined for inclusions inside quartz cement using a heating rate of 10°C/min (18°F/min) when the temperature was lower than 70°C (158°F) and a rate of 5°C/min (9°F/min) when the temperature exceeded

70°C (158°F). The measured temperature precision for Th is ±1°C (±1.8°F).

X-ray diffraction (XRD) analysis of whole-rock samples and quantitative clay minerals were performed on 65 core samples (32 samples from $T_3x^2$and 33 samples from T_3x^4) to identify species and contents of major minerals, relative contents of different clay minerals and I/S mixed-layer ratios. The whole-rock chemical analysis was performed on 65 sandstone samples for the content of major elements using direct-reading spectroscopy method of full spectrum (ICP-AES) under condition of 20□ temperature and 65% humidity. The rock samples were ground to fine powder and homogenized. Approximately 0.25 g of the powder was dissolved in a mixture of hot hydrofluoric and hydrochloric acids. The resultant solutions were diluted with distilled water before analysis. The solutions were analysed, using inductively coupled plasma atomic emission spectrometry (ICP), for aluminium, titanium, iron, manganese, calcium, magnesium, potassium and sodium (Gluyas and Coleman, 1992). Silicon was obtained by gravimetric methods. Precision on whole-rock analysis is estimated to be within +1% (Gluyas and Coleman, 1992).

4. Results

4.1 Sandstone petrography

The T_3x^2 sandstones mainly comprise litharenite and minor feldspathic litharenite, and the T_3x^4 sandstones consist of major litharenite and minor lithic quartz arenite（Fig. 3A-B,Table 1）.The sandstone classification was based on the standard of Folk et al., 1970 (Fig. 3A-B).The feldspars within the T_3x^2 and the T_3x^4 consist of plagioclase (major albite and minor calcic plagioclase) and K-feldspar (Table 1, Table 2). The rock fragments of the T_3x^2 and T_3x^4 sandstone mainly comprise fragments of major sedimentary rocks (e.g. limestone, dolomite and mudstone) , fragments of

metamorphic rock (e.g. phyllite, slate and shist) and small amounts of volcanic rocks (e.g. basalt and andesite).The T_3x^4 sandstones have more sedimentary and volcanic rock fragments and less detrital quartz than the T_3x^2 sandstones (Table 1). Carbonate rock including micrite limestone and dolomite is dominant in the sedimentary rock fragments of T_3x^2 and T_3x^4 sandstones. The T_3x^2 sandstones and T_3x^4 sandstones mainly comprise major medium-grained, minor fine-grained and 6.3% coarse-grained sandstones.

4.2 Diagenetic minerals and alterations

4.2.1 Compaction

Framework grains in the Xujiahe Formation sandstones (T_3x^2 and T_3x^4) are generally heavily compacted (both mechanically and chemically), as is indicated by the dominance of long and concave-convex grain contacts (Fig. 4A-F). Direct evidence of mechanical compaction, which has mostly occurred in the T_3x^4, are the deformation of mica and plastic rock fragments (Fig. 4A, B, E, F). Chemical compaction, pressure dissolution, observed in T_3x^2, is manifested by the concave–convex and sutured contacts between quartz grains (Fig. 8A-B, Fig. 4C, D). However, compaction is obviously less extensive in sandstones with chlorite rims than in other rocks within the T_3x^2 (Fig. 11G-I).

4.2.2 Carbonate cements

Carbonate cements are the dominant cement in the sandstones. They occur as scattered euhedral rhomb and pore-filling blocky and mosaic aggregates in the T_3x^2 and T_3x^4 tight sandstones (Fig. 5, Fig. 6). In the T_3x^2 tight sandstones, carbonate cements with an average of 6.68% mainly consist of calcite (av.vol 3.72%) and dolomite (av. vol 2.96%) (Table 1). The calcite generally occurs as isolated blocky sparite cements filling intergranular pores (pore diameter,50μm～120μm, (Fig. 5A)

and as partial replacements of detrital grains (e.g. feldspars and volcanic rock fragments, Fig. 5D, E). Dolomite also occurs as pore-filling poikilotopic sparite patches that fill intergranular pores (pore diameter, 50 μm～200 μm, Fig. 5B) or as euhedral rhomb (single crystal: 40μm～120μm) and partial replacements of detrital grains (e.g. feldspar) filling intragranular pores (Fig. 5D- F).

The carbonate cement has an average content of 5.92% in the T_3x^4 sandstones, of which 4.97% is calcite and 0.95% is dolomite (Table 1). Calcite cements mostly occur as microcrystallineto sparite (single crystal:10μm～50μm), poikilotopic masses that fills in primary (intergranular) pores (Fig. 6A-C), and as partial replacements of detrital grains (e.g. feldspars and rock fragments) that fill secondary pores (intergranular and intragranular dissolved pores) and accompany partial dissolution and kaolinization of feldspar (Fig. 6D-F). The minor (0.95%) sparite dolomite (single crystal:30μm～80μm) generally occur as partial replacements of detrital grains (e.g. carbonate rock fragments), and accompany the dissolution of carbonate rock fragments (Fig. 6D).

The primary and secondary intergranular pores, filled with calcite/dolomite cements, can be distinguished by thin-section analysis that were impregnated with blue epoxy resin or the scanning electron microscope analysis (SEM). The primary pores that are filled with calcite cement generally have regular edges which abut against the original detrital grains (Fig. 5A, Fig. 6A-B). However, the secondary intergranular pore is characterized by irregular edges that are formed by partial dissolution and replacement of calcite around the detrital grains (feldspar)(Fig. 6A-B). Feldspars that are partly replaced by calcite are generally accompanied by dissolution in the T_3x^2 and T_3x^4 sandstones (Fig. 5D-F-, Fig. 6D-F). CL micrographs show that the carbonate cements of the Xujiahe Formation sandstones can be divided into two

generations of early and late carbonate cement (Fig. 6B). The saffron yellow micro-crystal calcite that fills primary pores, which represent the first generation,precipitated before strong mechanical compaction as evidenced by the floating detrital grains and point contacts between grains (Fig. 6B). The orange red calcite that mostly fills the residual primary pore and secondary pores and partially replaced some detrital grains, represents the second generation (Fig. 6 B). The calcite cements of T_3x^4 sandstone consist of major early calcite and minor late calcite, but the T_3x^2 sandstone was dominated by late calcite.

Electron microprobe (EMP) analyses reveal the molar compositional fraction of carbonate cements in the T_3x^2 sandstone and the T_3x^4 sandstone (Table 4). The calcite cements have nearly similar molar compositional fraction between the T_3x^2 sandstone and the T_3x^4 sandstone (Table 4). Besides, almost all of dolomite cements occur in the T_3x^2 sandstones and rarely in the T_3x^4 sandstones (Table 4). The dolomite should be classified as the ankerite for abundant $FeCO_3$ (av. 20.86%, Table 4).

The $\delta^{18}O_{V\text{-}PDB}$ and $\delta^{13}C_{V\text{-}PDB}$ values of calcite cements in the primary pores are similar to that of the calcite rock fragments and that of carbonate rock fragments in the T_3x^4 sandstones (Fig. 7A, Table 5). The dolomite (ankerite) crystals filling in the secondary pores have lower $\delta^{18}O_{V\text{-}PDB}$ values and similar $\delta^{13}C_{V\text{-}PDB}$ values in comparison to that of the calcite in primary pores in the T_3x^4 sandstones (Fig. 7A, Table 5). The $\delta^{18}O_{V\text{-}PDB}$ and $\delta^{13}C_{V\text{-}PDB}$ values of calcite cements in the secondary pores are obviously more negative than that of other carbonate in the T_3x^4 sandstones (Fig. 7A, Table 5).

In the T_3x^2 sandstones, the $\delta^{18}O_{V\text{-}PDB}$ values and $\delta^{13}C_{V\text{-}PDB}$ values of calcite cements are similar to that of dolomite (ankerite) cements ((Table 6, Fig. 7B). The dolomite fragments have similar $\delta^{18}O_{V\text{-}PDB}$ values and slightly higher $\delta^{13}C_{V\text{-}PDB}$ values

(Table 6, Fig. 7B).

4.2.3 Quartz cements

Point counting of thin section, cathodoluminescence, and SEM analyses indicate that authigenic quartz is the second most abundant cement after carbonate. Quartz cements generally occur as syntaxial overgrowths (thickness 20μm to 120μm) that partially coat of detrital quartz grains (Fig. 8A-C, Fig. 8F) or as isolated pore-filling quartz crystal (Fig. 8D, E, Fig. 8G). Quartz overgrowths are usually accompanied by sutured (microstylolitic) quartz grains contacts (Fig. 8A, F, I). The isolated pore-filling authigenic quartz crystal are generally accompanied by the dissolution of feldspar and some illite (Fig. 8E, H), indicating that the isolated pore-filling quartz crystals are like to be related to the dissolution of feldspar (Hawkins, 1978; Worden and Morad,2000).

The quartz cement of the T_3x^2 sandstones has an average content of 2.16%, which represents 24.4% of the total cement content (Table 1). Moreover, the quartz cement content increases with increasing amounts of detrital quartz in the T_3x^2 sandstones (Fig. 9). In the T_3x^4 sandstones, quartz cement generally occurs as isolated pore-filling quartz crystals or syntaxial overgrowths (Fig. 8B, Fig. 8E-G); this quartz cement has an obviously low average content of 0.94%, which represents 13.2% of the total cement content (Table 1).

The homogenization temperatures of fluid inclusions in quartz cements reveal that crystallization temperature of quartz cements in the T_3x^2 sandstones ranges from 50 to 90℃, 100 to 140℃ and 150 to 190℃ and that those of the T_3x^4 sandstones mostly range from 90 to 150℃ (Fig. 10). In addition, the homogenization temperatures of aqueous inclusions in authigenic quartz within fractures range from 50 to 60℃ and 170 to 330℃.

4.2.4 Clay minerals

Illite, chlorite, kaolinite and minor mixed-layer illite/smectite (less than 1% of the clay minerals), were revealed by XRD and SEM analyses (Table 2, Table 3). Illite, which represents 46.8% (average) of clay mineral in T_3x^2 and 43%(average) in T_3x^4 sandstones, occurs mainly as grain-coatings, nested aggregates filling in secondary intragranular dissolved pores and non-netted aggregates filling in intergranular spaces (Fig. 11A-F, Meng et al., 2011). The nested illites are generally accompanied by the dissolution of feldspar and rock fragments (Fig. 11A, B, E, F); non-netsted aggregates may be related to the illitization of the matrix consisting of smectite (Fig. 11C, O). The T_3x^2 sandstones have a higher chlorite content (av. 2.4, whole rock %; av. 51.9 clay %) than the T_3x^4 sandstones (av. 1.6, whole rock %; av. 26.1 clay %) (Table 2, Table 3, Fig. 12, Fig. 13). Chlorite rims are partly well-developed in the T_3x^2 which can be observed under cross-polarizing light and SEM analysis (Fig. 11G-I). However, in the fourth member (T_3x^4), chlorite cement is dominated by authigenic pore-filling chlorite (Fig. 11K), and some chlorite appears as chloritized of rock fragments (Fig. 11J).

Kaolinite, which represents 0% to 72 % (av.28.5%) of all clay minerals, mostly occurs at the top of the T_3x^4 sandstones and is nearly absent in the T_3x^2 sandstones (Table 2, Table 3, Fig. 12, Fig. 13, Fig. 14B). Kaolinite generally occurs as vermicular or booklet-like aggregates of pseudohexagonal crystals (Fig. 11L~M). They are usually observed in secondary pores associated with feldspar dissolution (Fig. 11M). In addition, some booklet-like pseudohexagonal kaolinite has transformed into filamentous illite (Fig. 11N). Small amounts of flaky smectite are present in the mixed-layer illite/smectite (Table 4, Fig. 11O).

4.2.5 Dissolution

Secondary pores, which are the most important pore type in the studied sandstones, were generally formed by the dissolution of major feldspars and minor volcanic rock fragments (point counting) (Fig. 15A-F). Secondary pores mostly occur at the top of T_3x^4; others occur at the bottom of T_3x^4 and in the middle-upper part of T_3x^2 (Fig. 16). Overall, the dissolution is more prevalent in T_3x^4 than T_3x^2 sandstone (Fig. 4, Fig. 16). Detrital K-feldspar grains have experienced partial to complete dissolution (Fig. 15A-C). Feldspar dissolution is generally accompanied by the formation of some authigenic kaolinite and quartz (Fig. 11-M, Fig. 15B).

4.3 Pore types, porosity and permeability

The pore space of T_3x^2 sandstone consists of primary pore (av.0.84%), secondary dissolved pore (av.0.79%) and fracture (0.23%) (Fig. 17). The pore space of T_3x^4 sandstone comprises major secondary dissolved pore (av.3.49%), minor primary pore (av.0.58%) and fracture (0.09%) (Fig. 17).

The core porosity of T_3x^2 sandstone mainly ranges from 1% to 5% (av.3.44%), and the core permeability ranges from 0.02 to 0.16mD (av.0.089mD). In the T_3x^4 sandstones, core porosity generally characterized by two main ranges of 1%－3% and 3%－9% (av.5.14%), the core permeability ranges from 0.02 to 0.32mD (av.1.08mD).

In porosity-depth and permeability-depth profiles, both porosity and permeability of T_3x^2 and T_3x^4 sandstones show wide variation at shallow to deep depths (Fig. 18). Porosity and permeability generally decrease with increasing burial depth. However, porosity and permeability values of P10 (10% of reservoirs have porosity higher than this value) and P50 (median) curves show that some higher porosity and permeability intervals exist in the T_3x^2 and T_3x^4 sandstones (Fig. 18).

4.4 Sandstone geochemistry

The major elements (whole rock) of T_3x^2 sandstones and T_3x^4 sandstones comprise Na_2O, K_2O, MgO, Fe_2O_3, TiO_2, Al_2O_3, SiO_2 (Table S1, Table S2). The MgO, K_2O, Al_2O_3 contents of T_3x^4 sandstone have obvious vertical changes, but that of T_3x^2 sandstone present relatively fixed values in vertical profile (Fig. 12A, Fig. 13A).

5. Discussion

5.1 Mechanism and time of dissolution

The types of pore space and the porosity-depth and permeability-depth profiles indicate that the dissolution of minerals was the most important source of pore space creation in the T_3x^2 and T_3x^4 sandstones (Fig. 17, Fig. 18). For dissolution to occur the pore fluids need to be under saturated with respect to the detrital minerals. Under saturation can come about simply from increased temperature during burial or from a change in composition of the pore fluid caused ingress of new pore fluids. A candidate fluid that would promote dissolution is an acidic one and we know that organic acids would have been formed from the thermal maturation of coal in the adjacent T_3x^3 and T_3x^5 members.

Coal-bearing stratum produce many kinds of organic acids during early diagenetic stage (Kauss et al., 1997; Dias et al., 2002) and peak at temperature range of 80℃ to 140℃ (Surdam et al.,1989; Zeng et al., 2007). The amount of organic acids generated by coal-bearing strata (T_3x^3 and T_3x^5) is generally 2-5 times higher than other kinds of source rock (T_3x^1) (Zheng and Ying, 1997; Yuan et al.,2013). Feldspar dissolution, secondary pores and enlarged dissolution of micro-fractures are prevalent in the studied sandstones (Fig. 14, Fig. 15A-C,Fig. 15F,Fig .16,Fig. 17).Fig. 17, Besides, the distribution of secondary pore is related to source rocks (Fig. 16A-D).These indicate that acidic fluids from source rocks migrated and flowed into the T_3x^2 and T_3x^4

sandstones through these fractures, meanwhile provoked pervasive dissolution in studied sandstones (Fig. 15F). Hence, the feldspar dissolution of the T_3x^4 and T_3x^2 sandstones may occur from eodiagenesis to mesodiagenesis stage (60℃-140℃).

Secondary pores are mostly distributed on the top of T_3x^4, where they approximately correspond to the zone containing decreasing amounts of feldspars, the development of kaolinite and the skewness/rapid change of the Ro value, and more prevalent than the middle part of T_3x^4 (Fig. 14, Fig. 16)..Therefore, feldspar dissolution recorded at the top of the T_3x^4 might be caused by acidic fluids from the coal-bearing formation of the T_3x^5) . Besides, there is an extensive II-type unconformity on the top of the T_3x^4 (Zhang, 2011). As such some early dissolution might come from leaching by low-pH meteoric waters containing CO_2 gas phase .

However, there are not more secondary pores (Fig. 16A-D) and higher core porosity (Fig. 18A) at the bottom of T_3x^2 than there are in the middle-upper part, even if they are adjacent to the Xiaotangzi Formation (T_3x^1), which mainly consist of the source-rock (Fig. 2). This may be explained by the fact that obviously thinner sandstone, less feldspar, more alkaline diagenetic environment in the bottom of the T_3x^2 consisting of similar marine mudstone interbedded with sandstone than there is in the middle-upper part , which resulted in less feldspar dissolution in sandstones (Fig. 2). In addition, some few rock fragments (e.g. carbonate and volcanic rock fragments) were dissolved together with feldspars by these acidic fluids (Fig. 15D, E).

5.2 Genesis of diagenetic minerals

5.2.1 Source, temperature and time of carbonate diagenesis

Carbonate cements have many potential carbon sources including internal and external sources (Gier et al., 2008; El-Ghali et al., 2013; Luo et al.,2018). The

$\delta^{18}O_{water}$ values of parent diagenetic pore water of the calcites filling primary pores comprising the meteoric and marine water within the T_3x^4 are approximate -3‰ SMOW, and that of current pores water in the T_3x^4 range from-4.3‰ to +0.5‰ (SMOW) with an average value of -1.4‰ (SMOW) (Shen et al, 2010; Liu et al, 2014a,b). The $\delta^{18}O_{water}$ values of parent diagenetic pore water of carbonate cements in the T_3x^2, which was deposited in marine water, were nearly 0‰ SMOW, and the $\delta^{18}O_{water}$ values of current pore water range from -4.5‰ to -1.3‰(SMOW) (Shen et al, 2010;Liu et al, 2014a,b). Using oxygen isotope fractionation factor for calcite-water from Friedman and O'Neil (1977), the precipitation temperatures for different types of carbonate cements can be calculated (Table 5, Table 6, Fig. 18, Fig. 19).

The early calcite cements filling the primary pores of the T_3x^4 sandstone (-10.06‰ to -4.75‰, av. +7.38‰) were calculated to be precipitated at approximately 30-65℃ (Table 4, Fig. 19A). Moreover, nearly poikilotopic calcite cements filling in primary (intergranular) pores mostly occur as microcrystalline to sparite (Fig. 6A,C), which also indicate that calcite precipitated at the early diagenetic stage. The calcites filling the primary pores of the T_3x^4 sandstone have similar carbon and oxygen values ($\delta^{18}O_{V\text{-}PDB}$ -10.06 to -4.75‰, av. -7.38‰; $\delta^{13}C_{V\text{-}PDB}$: -0.13 to +2.46‰, av. 1.53‰) with those of carbonate rock fragments ($\delta^{18}O_{V\text{-}PDB}$ -9.23 to -4.81‰; $\delta^{13}C_{V\text{-}PDB}$ 1.33 to +2.22‰) (Table 5, Fig. 7A). These data provide evidence for that the carbon source of the early calcite cement filling the primary pores in the T_3x^4 sandstones is closely related to the internal carbonate rock fragments consisting of inorganic carbon whose $\delta^{13}C_{V\text{-}PDB}$ values can increase up to 3‰, and rarely related to the organic carbon/acid (Friedman and O' Neil, 1977). However, there was not enough acid for the dissolution of internal carbonate rock fragments at the early diagenetic stage (30-65℃). Therefore, the early calcite filling in the primary pores precipitated from pore fluids containing

Ca^{2+} and CO_3^{2-} come from the original formation water in sandstone and adjacent mudstone at eodiagenesis stage, which were mainly related to weathering or dissolution of carbonate rock fragments in the provenance or transport process.

The calcite cements filling in the secondary of the T_3x^4 sandstone ($\delta^{18}O_{V\text{-}PDB}$:-19.71‰ to -10.77‰, av.-14.69‰) pores were calculated to be precipitated at 70℃-160℃ (Table 5, Fig. 19A).. The measured $\delta^{13}C_{V\text{-}PDB}$ values (−5.43‰ ~ 0.75‰) show that this calcite may be related to the oxidation of organic carbon or formed under methanogenic conditions (Friedman and O' Neil, 1977; Irwin et al., 1977; Wei et al., 2015). Late-diagenetic calcite cements in the secondary pores are generally accompanied by the dissolution of feldspars and some rock fragments (e.g. carbonate rock and volcanic rock fragments)(Fig. 6D~F). Therefore, material sources of the calcite cements filling in the secondary pores is closely related to the late dissolution caused by organic acids from thermal evolution of organic matter in the source rocks. In addition, the transformation of clay minerals may also supplied some Ca^{2+}, Fe^{2+} and Mg^{2+} at the temperature range of 80℃to 140℃.

The $\delta^{13}C_{V\text{-}PDB}$ values (−0.97‰ ~ +1.97‰) of the small amounts of dolomite (ankerite) filling in the secondary pores are somewhat less than those of carbonate rock fragments in the T_3x^4 sandstones (Fig. 7A) and more than those of organic carbon. This suggests that the carbon source of dolomite cement may be the mixture of organic carbon and carbonate rock fragments. In addition, the relatively high precipitation temperature (75℃-140℃) (Table 5, Fig. 19B) of dolomite (ankerite) cements is consistent with the temperature of release of organic acid and CO_2 from the source rock within T_3x^3 and T_3x^5 (Fig. 2) (Surdam et al,1989; Zeng et al, 2007). Besides, the polycrystalline dolomite (ankerite) (30μm～80μm) generally occurs as partial replacements of detrital grains (e.g. carbonate rock fragments) and accompany

the dissolution of carbonate rock fragments (Fig. 6D). Therefore, the dolomite (ankerite) cements within the T_3x^4 sandstones may have mainly precipitated from the dissolution of carbonate rock fragments by organic acids during mesodiagenetic stage (75℃-140℃).

In the T_3x^2 sandstones, the relatively positive $\delta^{13}C_{V\text{-}PDB}$ values (-1.81‰ to +4.97‰) suggest that these carbonate cements (calcite and dolomite) were mainly formed under methanogenic conditions (Table 6, Fig. 7B) (Irwin et al., 1977; Wei et al., 2015). The calcite and dolomite cements precipitated at 70℃-120℃and 80℃-160℃ respectively (Table 6, Fig. 20A), which were equivalent to the mesodiagenetic stage. Concurrently, the source rock in the lower submember of T_3x^2 and the underlying Xiaotangzi Formation (T_3x^1) exists under methanogenic conditions. Carbonate cements have mainly developed in the lower submember of the T_3x^2, which is adjacent to the underlying Xiaotangzi Formation, which consists of marine source rocks (Fig. 2, Liu et al, 2014b; Luo, 2015), which can be explained by the fact that the organic acid within mudstone intruded into the sandstone. Therefore, carbon sources of carbonate cements (late diagenetic carbonate cements) in the T_3x^2 could have come from the organic acids that flowed into sandstone from the source rock. The Ca^{2+}, Fe^{2+} and Mg^{2+} may come from late dissolution of feldspar and rock fragments, transformation and interstitial water of clay minerals and reduction of iron oxides.

5.2.2 Source, temperature and time of authigenic quartz

Quartz cements are usually accompanied by sutured (microstylolitic) contacts of quartz grains formed by pressure dissolution (Fig. 8A, Fig. 8I), and increasing quartz cement content with increasing detrital quartz content in the T_3x^2 sandstones (Fig. 9). However, pressure dissolution is rare in the T_3x^4 sandstones, due to their low contents of detrital quartz grains. Therefore, pressure dissolution represents the most important

silica source for quartz cement in the T_3x^2 sandstones (Luo et al., 2015), but not in the T_3x^4 sandstones.

The isolated pore-filling authigenic quartz crystals are generally accompanied by the dissolution of feldspar in the T_3x^2 and T_3x^4 sandstones (Fig. 8G-H). Therefore, feldspar dissolution, which was pervasive and might occur from eodiagenesis to mesodiagenesis stage (60℃-140℃), may be an important source for the quartz cements. The 80°C ~120°C is the ideal temperature range for feldspar dissolution (Surdam et al., 1989).The homogenization temperatures range (90°C and 120°C) of fluid inclusions in quartz cements of the T_3x^4 sandstones (Fig. 10A) also suggest that the quartz cements may be mainly derived from the feldspar dissolution the T_3x^4 sandstones. However, the homogenization temperature range (90°C and 110°C) in the T_3x^2 sandstones are nearly absent (Fig. 9B). Moreover, the higher residual feldspar content of the T_3x^2 sandstones (av. 8.3 vol%) than the T_3x^4 sandstones (av.2.1vol%) (Table 1, Table 2, Table 3, Fig. 3A-B) and the less secondary pores of the T_3x^2 sandstones than the T_3x^4 (Fig. 17) may also indicate that feldspar dissolution may be not the most important silica source for the quartz cements in the T_3x^2 sandstones.

The type and content of clay minerals suggest that extensive clay mineral transformation occurred in the T_3x^2 and T_3x^4 sandstones (Table 2, Table 3). The nested illites related to feldspar dissolution (Fig. 11A, B, E, F), non-netsted aggregates related to the illitization of smectite (Fig. 11C, O), some filamentous illites transformed from booklet-like pseudohexagonal kaolinite (Fig. 11N) and chlorite rim (Fig. 11G-K) were the results of clay mineral transformation. Symbiotic relationship of quartz cement and authigenetic clay minerals indicates that the clay mineral transformation is the potential source for quartz cements (e. g. illite and chlorite) (Fig. 8E, Fig. 11I). Moreover, the homogenization temperatures range (110℃ to 140℃) of

quartz cements (Fig. 10A-B) is in favour of the clay minerals transformation (Worden and Morad, 2003). These indicate that clay mineral transformation within the sandstone might be one of silica sources for quartz cements in the T_3x^2 and T_3x^4 sandstones.

Quartz cements with homogenization temperatures between 50℃ and 90℃ comprise 40% of total T_3x^2 sandstone samples,but represent just 5% of total T_3x^4 sandstone samples (Fig. 10A, B). However, the feldspar dissolution of T_3x^4 sandstone is more pervasive than the T_3x^2 sandstones indicate that (Fig. 16, Fig. 17). Furthermore, some authigenic quartz located in fractures have homogenization temperatures varying from 50℃ to 60℃ in the T_3x^2 sandstones. Therefore, the external silica source at eodiagenesis stage (50-60℃), which might be related to the oversaturated fluid derived from mudrocks through fractures,may be one of important silica sources for quartz cement in sandstones, especially in the T_3x^2 sandstones (Gluyas and Coleman, 1992; Gluyas et al, 2000; Luo et al.,2015).

In addition, the presence of some quartz cement filling in fractures with homogenization temperatures ranging from 210℃ to 290℃ suggests that hot fluids moving up through fractures could represent another possible external source. However, the homogenization temperatures of the quartz cements filling these pores rarely reach 200℃, which may indicate that hydrothermal fluids with high temperatures and concentrations was not an important silica source for quartz cements in the T_3x^2 and T_3x^4 sandstones.

5.2.3 Temperature and time of clay mineral transformation

Clay-mineral assemblages generally transform with increasing temperatures, producing a series of prograde diagenetic reactions (Worden and Morad, 2003). Clay mineral transformations in the studied sandstones include kaolinitization and

illitization of feldspar (Fig. 11F, M), illitization and chlorization of smectite (Fig. 11O), conversion of kaolinite into illite and chlorite (Fig 11-N), and replacement of rock fragments by mesogenetic illite and chlorite (Fig. 11B, E, J).

The illitization of kaolinite is prevalent at temperatures greater than approximately 70°C, but becomes pervasive at temperatures greater than approximately 130°C in neutral or alkaline environments (Worden and Morad, 2003). When the temperature is above 120-140℃, the early kaolinite released by the feldspar dissolution can translated into illite with the K^+ from the K-feldspar dissolution (Chuhan and Bjørlykke, 2000; Zhang, 2011).

The nested illites and kaolinite are related to feldspar dissolution in the T_3x^2 and T_3x^4 sandstones (Fig. 11A, F, M, Fig. 14, Fig. 16). The K-feldspar contents have negative correlations with contents of illite (in whole rock and clay minerals) but positive correlations with chlorite in T_3x^2 sandstones (Fig. 12, Fig. 21E-F). Almost all the feldspar had been dissolved in T_3x^4 sandstones (Table 3, Fig. 13). The relative contents of kaolinite decrease with increasing content of illite and chlorite in the clay minerals of T_3x^4 sandstone (Fig. 13, Fig. 22F-J). The K_2O contents have positive correlations with illite contents (in whole rock but not clay minerals) in T_3x^2 and T_3x^4 sandstones (Fig. 21J-K, Fig. 22D-E). The illitization of potassium feldspar is widely observed in the T_3x^2 sandstone and T_3x^4 sandstone (Fig. 11A, F, M). These indicate that K-feldspar dissolution coincided with, and provided the necessary K^+ and kaolinite for, the illitization of kaolinite in the T_3x^2 and T_3x^4 sandstones (Fig. 21E-H, Fig. 22D-F).

Fig. 10Fig. 10Fig. 9Fig. 10Therefore, the kaolinite formed by feldspar dissolution have generally transformed into the illite or chlorite (Fig. 11N) at the mesodiagenetic stage with deep burial (Fig. 12, Fig. 13) (Worden and Morad, 2003,

Chuhanand Bjørlykke, 2000; Zhang, 2011). However, the pervasive kaolinite on the top of T_3x^4 formed by the dissolution and kaolinitization of feldspar (Fig. 11M), was preserved in the relatively deep burial depth (3000-4000 m) (Fig. 13, Fig. 14).This might be related to acidic condition due to top unconformity (Morad et al., 2000; Worden and Morad, 2003; Mansurbeg et al., 2006; El-ghali et al., 2006; Morad et al., 2012).

Almost all smectite has been transformed to illite or chlorite with the deep burial and heating of the T_3x^2 and T_3x^4 sandstones (Fig. 11O) (Table 2, Table 3). The negative correlation between K-feldspar and illite (Fig. 12) suggests that dissolution of K-feldspars might provide K^+ for illitization of smectite. Thus, some illite occurring as non-netted aggregates may have formed by the illitization of smectite and the dissolution of K-feldspars.

The chloritization of smectite is a dissolution–reprecipitation process that requires a pH-alkaline fluid and a source of aluminium, iron and magnesium, which may come from the alkaline dissolution of basic volcanic fragments (Chang et al., 1986). The early authigenic chlorite rims, which mostly occurs in the middle and lower part of T_3x^2 sandstones, increase with increasing K-feldspar content and decreasing illite content (Fig. 21I), indicate that chloritization was related to alkaline environment but not acidic dissolution of K-feldspar. The T_3x^2 sandstones contain relatively more volcanic fragments than the T_3x^4 sandstones and are adjacent to the Xiaotangzi Formation (equivalent to T_3x^1) (Fig. 2), which was deposited in a marine environment and is characterized by slightly alkaline waters (i.e., seawater pH is 8.3) (Worden and Morad, 2003). Besides, some chlorite occurs as replacement of volcanic rock fragment accompanying by the dissolution of rock fragments (Fig. 11J, K). Therefore, early authigenic chlorite rims of T_3x^2 sandstones were mainly formed by

the chloritization of eogenetic smectite (Fig. 12C) at eogenetic stage. Meanwhile, the alkaline dissolution of volcanic rock fragment provided the Mg^{2+} and Fe^{2+} for chloritization.

The pore-filling chlorite in the T_3x^4 sandstones, increase with decreasing kaolinite content and increasing illite content (Fig. 22H). These pore-filling chlorites may be related to the subsequent chloritization of kaolinite at eodiagenesis and early mesodiagenesis (Fig. 13C, Fig. 22G).The early acidic dissolution of volcanic rock fragment and feldspar provides the Mg^{2+} , Fe^{2+} and kaolinite for chloritization of kaolinite.

5.3 Mechanism and time of compaction

Compaction is the most important factor controlling the reservoir quality of the Xujiahe Formation sandstones (Huang et al., 2009; Meng et al., 2013). Although the burial depths of the T_3x^2 and T_3x^4 sandstones differ by approximately 1000 m, differences of degree in mechanical compaction are not so obvious, and even the mechanical compaction in the T_3x^4 sandstones is stronger than that in the deeper T_3x^2 sandstones (Fig. 4). Moreover, the pressure dissolution (chemical compaction), which generally occur at late mesodiagenesis, is more prevalent in T_3x^2 than it is in T_3x^4. This abnormal phenomena can be interpreted by these facts: first, the abundances of rock fragments (25%–75%, av. 40.8 vol %) are always higher in T_3x^4 sandstones than they are (17%–30% ,av. 21.7 vol %) in T_3x^2 sandstones (Table 1); second, the early chlorite rim, which plays an important role in the preservation of primary pores, is distributed mostly in the T_3x^2 sandstones but rarely in T_3x^4;third,the T_3x^2 sandstones contain significantly more detrital quartz (63.3–80% ,av. 70 vol%) than T_3x^4 (quartz, 25–70% ,av. 57.1 vol %) (Table 1). These may play an important role in the fact that the T_3x^2 sandstone have more primary pore (av.0.84%) and less

secondary dissolved pore (av.0.79%) than the T_3x^4 sandstone (secondary pore: av.3.49%, primary pore: av.0.58%) (Fig. 17).

5.4 Digenetic sequence and porosity evolution

Petrographic evidence observed in thin section, scanning electron microscope (SEM) and cathodoluminescence (CL) analysis can be used to decipher the relative diagenetic sequence in the study area. Moreover, the formation temperatures of authigenic minerals, which can be measured from aqueous inclusions or calculated using oxygen isotopic values can be used to infer a more accurate relative timing of the different diagenetic reactions. In summary, synthesizing petrographic observations, homogenization temperatures of fluid inclusions, isotopic analysis and source and mechanism of diagenesis can reconstruct the diagenetic history of the T_3x^2 and T_3x^4 tight sandstones, which is illustrated in Fig. 23 and Fig. 24, in which the burial and thermal histories are based on the results of previous studies (Zhang et al., 2002). On the basis of the diagenetic sequence and previous studies, which indicate the timing of tightness of T_3x^2 and T_3x^4 sandstones (Luo, 2015), the porosity evolution of the T_3x^2 and T_3x^4 tight sandstones were reconstructed in Fig. 23 and Fig. 24.

5.5 The characteristics, evolution and controlling factors of diagenetic (geochemical) system

5.5.1 Mass balance/transfer and evolution of diagenetic (geochemical) system

The K_2O content has a weakly positive correlation with absolute and relative content of illite (in whole rock and clay minerals) in the T_3x^2 sandstones (Fig. 21G-H) and but obviously positive correlation with absolute content of illite (in whole rock but not clay minerals) in the T_3x^4 sandstone (Fig. 22D-E). Besides, the K_2O content was nearly stable in the vertical profile of T_3x^2 sandstone but changeable in the vertical profile of T_3x^4 sandstone (Fig. 12，Fig. 13). The K_2O content should be

controlled by the fixed composition of parent rock but not the authigenetic illite (in whole rock) in a closed sandstone system without loss and export of K^+. Furthermore, the previous research suggests that the T_3x^4 have exported abundant K^+, but the T_3x^2 slightly exported K^+ (Shen et al., 2010). These suggest that the K-feldsapar dissolution provided the K^+ for subsequent illitization with abundant loss of K^+ in the T_3x^4 and little loss of K^+ in T_3x^2 sandstone systems at the early diagenetic stage (eodiagenesis and early mesodiagenesis) (Fig. 25A, B).

The dissolution of volcanic rock fragment provided the Mg^{2+} and Fe^{2+} for chloritization and dolomite cementation in T_3x^2 and T_3x^4 sandstone. The MgO content has a negative correlation with absolute content of chlorite (in whole rock) but a very weak negative correlation with relative content of chlorite (in clay minerals) in the T_3x^4 sandstone, which indicate the dissolution of volcanic rock fragment provided Mg^{2+} for authigenetic chlorite with significant loss of Mg^{2+} in an open system at early diagenetic system (Fig. 24, Fig. 25A). The MgO content has a weak correlation with absolute content of chlorite (in whole rock) but a negative correlation with relative content of chlorite (in clay minerals) in the T_3x^2 sandstones (Fig. 21B-C), which indicate alkaline dissolution of volcanic rock fragment provided Mg^{2+} for the early authigenetic chlorite with little loss of Mg^{2+} at early diagenetic stage (Fig. 23, Fig. 25B). The content of MgO (in whole rock) increase with the increasing dolomite (in whole rock) in the T_3x^2 and T_3x^4 sandstone (Fig. 21A,Fig. 22A),which suggests that the dissolution of volcanic rock fragment provided all the Mg^{2+} for the dolomite cement without significant export of Mg^{2+} at mesodiagenesis in the T_3x^2 and T_3x^4 closed sandstone system (Fig. 25A, B).

The contents of K_2O, MgO, Al_2O_3 in T_3x^4 sandstone have more obvious vertical changes than T_3x^2 sandstone (Fig. 12, Fig. 13). Moreover, feldspar dissolution and

related secondary pores in the T_3x^4 sandstone are obviously more pervasive than T_3x^2 sandstone (Fig. 15, Fig. 16, Fig.17, Table 2, Table 3). However, the content of quartz cement in T_3x^4 sandstone (av.0.94%) is obvious less than T_3x^2 sandstone (av.2.16%)(Table 1).Fig. 15These indicate that the T_3x^4 sandstone has ever experienced a more open geochemical system than T_3x^2 sandstone during the feldspar dissolution process at the eodiagenesis and early mesodiagenesis (Fig. 25A, B). Besides, the large amount of factures, enlarged dissolution of the micro-fractures and some quartz cement filling in fractures indicate that the focused fluid flow on fractures also represent partially more open systems during burial process in T_3x^4 sandstone and T_3x^2 sandstone (Fig. 15F, Fig. 25) (Zhang, 2005; Zeng, 2010; Luo,2015; Bjørlykke and Jahren, 2012).

5.5.2 Controlling factors on the diagenetic (geochemical) system

The deltaic setting and subsequent uplift and development of an unconformity controlled the early digenetic history of the sandstones when at shallow burial depth. Subsequent deep burial depth and tectonism drove the diagenetic alterations in the tight sandstone diagenesis system, because they accelerated diagenetic alterations by increasing the formation pressure and paleotemperature and produced abundant fractures (Fig. 23, Fig. 24).

5.2.3 Impacts on the reservoir quality of diagenetic (geochemical) system

Diagenetic modifications alter the types, amount and distribution of pore spaces, creating smaller and more disconnected pores (Lai et al., 2018a; Lai et al., 2018b). The diagenetic reactions, particularly the dissolution, generally result in significant changes in the sediment composition (e.g. K^+, Mg^{2+} and slica) (Fig. 12,Fig. 13, Fig. 21,Fig. 22) and formation of secondary pores in the open diagenetic (geochemical) system during near-surface , eodiagenesis and even early mesodiagenesis stage (Fig.

16, Fig. 17, Fig. 23, Fig. 24, Fig. 25A-B).. Besides, the T_3x^4 sandstone has ever experienced a more open geochemical system than T_3x^2 sandstone at the eodiagenesis and early mesodiagenesis (Fig. 25A, B). Therefore, the T_3x^4 sandstone produced more early calcite cements, kaolinite and secondary pores than T_3x^2 sandstone in the open diagenetic system at eodiagenesis and early mesodiagenesis (Fig. 15, Fig.17, Table 1, Table 2).

When the geotemperature is above 120-140℃that determined by burial depth, the early kaolinite released by the feldspar dissolution can translated into the illite with the K^+ from the K-feldspar dissolution (R1and R2), which can merge into one reaction (R3)(Chuhan et al., 2000; Zhang, 2011). The little amount of residual acids at eodiagenesis stage can trigger the illitization of K-feldspar (R3). Hence, the illitization of K-feldspar were controlled by the relative ratio of K-feldspar to kaolinite in closed geochemical system (Chuhan and Bjørlykke, 2000; Huang et al., 2009). The reaction for illitization of K-feldspar (R3) will produce 10.7% secondary space volume (Huang et al.,2009).

$$2KAlSi_3O_8\text{（K-feldspar）}+2H^+ + H_2O = Al_2Si_2O_5(OH)_4\text{（kaolinite）} + 4SiO_2 + 2K^+ \quad (R1)$$

$$3Al_2Si_2O_5(OH)_4\text{（kaolinite）} + 2K^+ = 2KAl_3Si_3O_{10}(OH)_2\text{（illite）} + 2H^+ + 3H_2O \quad (R2)$$

$$KAlSi_3O_8\text{（K-feldspar）} + Al_2Si_2O_5(OH)_4\text{（kaolinite）} = KAl_3Si_3O_{10}(OH)_2\text{（illite）} + 2SiO_2 + H_2O \quad (R3)$$

The ratio of kaolinite to K-feldspar in the T_3x^4 sandstone exceeded 1, so almost all the K-feldspar and part of kaolinite had translated into illite (Table 3). Whereas, the ratio of kaolinite to K-feldspar in the T_3x^2 was less than 1, so almost all the kaolinite and part of K-feldspar had translated into illite (Table 2) (Chuhan and Bjørlykke, 2000). Consequently, the illitization of K-feldspar (R3) in the T_3x^4 sandstone produced more secondary pores than T_3x^2 sandstone in closed geochemical system during mesodiagenesis (Fig. 25).

The strong mechanical and chemical compaction (pressure dissolution) of the T_3x^2 and T_3x^4 tight sandstone destroyed most of the primary pores and some secondary pores (Fig. 4, Fig. 25A-B). The early secondary pore formed in open system may be destroyed by subsequent compaction. However, the associate kaolinite, which was generally formed by early feldspar dissolution in open system, will determine the late effective secondary pores by influencing late illitization of K-feldspar (R3) at mesodiagenesis (Fig. 25). Therefore, the average secondary thin-section porosity of T_3x^4 sandstone (av.3.49) is obviously higher than T_3x^2 sandstone (av.0.79%) (Fig. 4). The average primary porosity of T_3x^2 sandstone (av.1.09%) is higher than the T_3x^4 sandstone(av.0.58%), because grain-coating clay minerals (chlorite rim and illite coating) of T_3x^2 sandstone help to preserve porosity at depth by retarding compaction in the relatively closed system (Fig.11I,K,Fig. 25)(Luo et al.,2019). However, the pore space was dominated by secondary dissolution pores in the T_3x^2 sandstone and T_3x^4 sandstone, and both core porosity and permeability of T_3x^4 sandstone are therefore obviously higher than the T_3x^2 sandstone (Fig. 18, Fig. 25). The late diagenesis (late carbonate and quartz cementation) of the T_3x^2 and T_3x^4 sandstone, which were related to the dissolution and precipitation, produce no significant change of composition and porosity in nearly closed system at the late diagenetic stage. Therefore, the diagenetic characteristics and evolution of diagenetic systems can be used to predict about the reservoir quality based on the burial history, tectonic activities and certain primary sediment composition related to delta facies and provenance (Fig. 25A-B).

6. Conclusions

This study of the upper Triassic Xujiahe Formation in the Western Sichuan foreland basin, China, yields important clues about the diagenetic characteristics, size,

evolution and controlling factors of the diagenestic (geochemical) system and their impacts on reservoir quality in the tight deltaic sandstone, including the following:

1. Tight deltaic sandstones have undergone a significant and complicated series of diagenetic modification.

2. The strong compaction and carbonate cementation destroyed almost all the primary pores. The feldspar dissolution was the most important source of pore space in the T_3x^2 and T_3x^4 sandstones.

3. The T_3x^4 sandstone with significant loss of K^+, Mg^{2+} and silica experienced a more open diagenetic (geochemical) system than the T_3x^2 sandstone at near-surface, eodiagensis and early mesodiagenesis stage.

4. The T_3x^4 sandstone produced more early calcite cements, kaolinite and secondary pores than T_3x^2 sandstone in the open diagenetic system at eodiagenesis and early mesodiagenesis (Fig. 4, Fig.16, Table 1, Table 2).

5. Both the T_3x^2 and T_3x^4 sandstone represent nearly closed diagenetic (geochemical) system during middle-late mesodiagenesis. The late dissolution and illitization of K-feldspar, which was controlled by the parent composition (e.g. K-feldspar) and diagenesis in early open system (e.g. remaining kaolinite, K^+, K-feldspar and acids), was the main pore sources in the closed system.

7. Acknowledgements

The authors gratefully thank the editor and the reviewers for their valuable comments. Moreover, we specially thank Research Institute of Petroleum Exploration & Development, Southwest Oil-Gas Branch Company of Sinopec for providing all the related core samples and geological data. This study was jointly supported by the Major Special Project for National Science and Technology [Grant numbers.

2016ZX05033-001-002], the National Natural science Foundation of China [Grant numbers. 41202043] and the China Scholarship Council (CSC).

References

Bjørlykke, K., 2010, Petroleum geoscience: From sedimentary environments to rock physics: New York, Springer Verlag, 508 .

Bjørlykke, K.,2011. Open-system chemical behaviour of Wilcox Group mudstones. How is large scale mass transfer at great burial depth in sedimentary basins possible? A discussion.Mar. Petrol. Geol. 28, 1381–1382.

Bjørlykke, K., 2014. Relationship between depositional environments, burial history and rock properties. Some principal aspects of diagenetic process in sedimentary basins. Sediment. Geol. 301, 1-14.

Bjørlykke, K., Jahren, J., 2012. Open or closed geochemical systems during diagenesis insedimentary basins: constraints on mass transfer during diagenesis and the prediction of porosity in sandstone and carbonate reservoirs. AAPG Bull. 96, 2193–2214.

Boles, J, R., Franks, S, G., 1979. Clay diagenesis in Wileox sandstones of southwest Texas:implications of smeclite diagenesis on sandstone cementation.J. Sediment Petrology.49, 55-70.

Chang, H.K., Mackenzie, F.T. Schoonmaker, J., 1986. Comparisons between the diagenesis of dioctahedral and trioctahedral smectite, Brazilian offshore basins. Clay Miner. 34, 407–423.

Chuhan,F.A., Bjørlykke, K.,2000.The role of provenance in illitization of deeply buried reservoir sandstones from Haltenbanken and north Viking Graben, offshore Norway. Mar. Pet. Geol.17, 673-689.

Clark, S.J., 2014. Constraining diagenetic timings, processes and reservoir quality in igneous-affected basins, Durham theses, Durham University. Available at Durham E-Theses Online: http://etheses.dur.ac.uk/10827/.Curtis, C, D., 1978. Possible link between sandstone diagenesis and depth-ralate geochemical reactions occurring in enclosing mudstone.J. Geol. Soc.Lond135,107-114.

Day-Stirrat, R.J., Milliken, K.L., Dutton, S.P., Loucks, R.G., Hillier, S., Aplin, A.C., Schleicher,

A.M., 2010. Open-system chemical behavior in deep Wilcox Group mudstones, Texas Gulf Coast, USA. Mar. Pet. Geol. 27, 1804-1818.

Day-Stirrat, R. J., K. L. Milliken, S. P. Dutton, R. G. Loucks, S. Hillier, A. C. Aplin, and A. M. Schleicher, 2011, Discussionin response to Knut Bjørlykke regarding JMPG_1376 "Open-system chemical behavior in deep Wilcox Group mudstones, Texas Gulf Coast, U.S.A". Mar. Pet. Geol. 28, 1383–1384.

Dias, R. F., Freeman, K. H., Lewan, M. D., Franks, S. G., 2002. $\delta^{13}C$ of low-molecular weight organic acids generated by the hydrous pyrolysis of oil-prone source rocks. Geochimica Cosmochimica Acta. 66 (15), 2755–2769.

El-Ghali,M,A,K., El Khoriby,E,., Mansurbeg,H., Morad,S., Ogle,N.,2013., Distribution of carbonate cements within depositional facies and sequence stratigraphic framework of shoreface and deltaic arenites,Lower Miocene, the Gulf of Suez rift, Egypt .Mar. Pet. Geol.45, 267-280.

El-ghali,M,A,K., Tajori,K,G., Mansurbeg,H.,2006. The influence of transgression and regression on the spatial and temporal distribution of diagenetic kaolin in the Upper Ordovician glaciogenic sandstones within a sequence stratigraphic framework, Murzuq Basin, SW Libya. J. Geochem. Explor.89, 87-91.

Friedman, I., O'Neil, J.R., 1977. Data of Geochemistry: Compilation of Stable Isotope Fractionation Factors of Geochemical Interest [M]. US Government Printing Office.

Folk, R. L., 1980. Petrology of Sedimentary Rocks. Hemphill Publishing Co., Austin, Texas.

Gier, S., Worden, H.R., Johns, D.W., Kurzweil, H., 2008. Diagenesis and reservoir quality of Miocene sandstones in the Vianna Austria. Mar. Petrol.Geol. 25,681-695.

Gluyas, J., Coleman, M., 1992. Material flux and porosity changes during sediment diagenesis Nature: 356, 52-54.

Gluyas, J.G.,1997. Poroperm Prediction for Reserves Growth Exploration: Ula Trend Norwegian North Sea, AAPG Memoir 69, 201-210.

Gluyas, J. G., Witton, T., 1997. Poroperm prediction for wildcat exploration prospects, Miocene Southern Red Sea, AAPG Memoir, 69, 163-176.

Gluyas, J.G., Garland, C.R., Oxtoby, N.H. and Hogg, A.J.C. (2000) Quartz cement; the Miller's

tale In Special Proceedings Vol 29, International Association of Sedimentologists (eds R. H.Worden and S Morad) 199-219

Hansen, H, N., Løvstad, K., Müller, R., Jahren, J.,2017. Clay coating preserving high porosities in deeply buried intervals of the Stø Formation. Mar. Pet. Geol.88,648-658.

Hawkins, P.J., 1978.Relationship between diagenesis, porosity reduction, and oil emplacement in late Carboniferous sandstone reservoirs, Bothamsall oilfield, east Midlands. Journal of Geological Society. 135, 7–24.

Huang,S.,Huang,K.,Feng,L.,Tong,H.,Liu,L.,Zhang,X.,2009.Mass exchanges among feldspar, kaolinite and illite and their influences on secondary porosity formation in clastic diagenesis-A case study on the Upper Paleozoic, Ordos basin and Xujiahe Formation,Western Sichuan depression.Geochimica.38(05),498-506(in Chinese with English Abstract).

Irwin, H., Curtis, C., Coleman, M., 1977. Isotopic evidence for source of diagenetic carbonates formed during burial of organic-rich sediments. Nature. 269, 209–213.

Kauss, K.G., Copenhaver, S.A., Braun, R.L., Burnham, A.K., 1997. Hydrous pyrolysis of New Albany and Phosphoria Shales: production kinetics of carboxylic acid and light hydrocarbons and interactions between the inorganic and organic chemical systems. Org. Geochem. 27 (7/8), 477–496.

Lai, J., G. Wang, Y. Ran, and Z. Zhou, 2015, Predictive distribution of high quality reservoirs of tight gas sandstones by linking diagenesis to depositional facies: Evidences from Xu-2 sandstones in Penglai area of central Sichuan basin, China. J. Nat. Gas. Sci. Eng.23, 97–111.

Lai, J., Wang, G., Wang, Z., Chen, J., Pang, X., Wang, S., Zhou, Z., He, Z., Qin, Z., Fan, X.,2018a. A review on pore structure characterization in tight sandstones: Earth Sci. Rev. 177, 436-457.

Lai, J., Wang, G., Cao, J., Xiao, C., Wang, S., Pang, X., Dai, Q., He, Z., Fan, X., Yang, L., Qin, Z.,2018b. Investigation of pore structure and petrophysical property in tight sandstones. Mar. Pet. Geol. 91, 179-189.

Lin, L., 2005. Sedimentary Facies and Paleogeographic Evolution of the upper Triassic Xujiahe Formation in West Sichuan Foreland. (master thesis) Chengdu university of technology, Chengdu, Sichuan, China.21-40(in Chinese with English Abstract).

Liu, S., 2010. Research on Origin of Fluid and Gas Dynamic Accumulation Characteristics of

Xujiahe Formation in the Middle Member of West Sichuan Depression. (doctor thesis) Chengdu university of Technology, Chengdu, Sichuan, China (in Chinese with English Abstract).

Liu, S., Shen, Z., Lv, Z., Wang, P., 2014a.Characteristics and porosity evolution of relatively high-quality reservoirs of T_3x^4 in Xinchang area, Sichuan, China. Journal. Chengdu University Technology (Science and Technology Edition).41(04), 428-436 (in Chinese with English abstract).

Liu, S., Huang, S., Shen, Z., Lv, Z., Song, R.,2014b. Diagenetic fluid evolution and water-rock interaction model of carbonate cements in sandstone: An example from the reservoir sandstone of the Fourth Member of the Xujiahe Formation of the Xiaoquan-Fenggu area, Sichuan Province, China.Science China: Earth Sci. 57, 1077–1092(in Chinese with English abstract).

Luo, L., Meng, W., Feng, M., Tan, X., Zhang, S., Sun, S., Xiao, C., 2015. Silica sources of quartz cements and its effects on the reservoir in tight sandstones: A case study on the second member of the Xujiahe Formation in Xinchang structural belt, western Si-chuan depression. Natl Gas Geosci. 26(03), 435-443(in Chinese with English abstract).

Luo, L., 2015.Research on diagenetic facies of the 2nd member of Xujiahe Formation in the Xinchang structural belt. (master thesis) Chengdu university of Technology, Chengdu, Sichuan, China (in Chinese with English Abstract).

Luo, L., Gao,X., Meng,W., Tan,X., Shao ,H., Xiao, C.,2018. The origin and alteration of calcite cement in tight sandstones of Jurassic Shishugou Group in the Fukang Sag, Junggar Basin, NW China: Implications for fluid–rock interactions and porosity evolution. Aust. J. Earth. Sci. 65(3), 427-445.

Luo,L., Gao,X., Gluyas,J., Tan,X., Cheng,C., Kong,X., Qu,F., Shao,H.,2019. Reservoir quality prediction of deeply buried tight sandstones in extensively faulted region: A case from the Middle-Upper Jurassic Shishugou Group in central Junggar Basin, NW China. J. Petrol. Sci. Eng. 175, 22–45.

Luo, L., Gao, X., Meng, W., Tan, X., Feng, M., Shao, H., 2017. The Formation Mechanism of the Relatively High-quality Reservoir in Tight Sandstones with Deep Burial: A Case Study of

Xujiahe Formation in Xinchang Structural Belt of Western Sichuan Depression. Acta Geoscientica Sinica.38(6),930-944 (in Chinese with English Abstract).

Mansurbeg,H., El-ghali,M,A,K., Morad,S., Plink-Björklund,P.,2006. The impact of meteoric water on the diagenetic alterations in deep-water, marine siliciclastic turbidites. J. Geochem. Explor.89, 254-258.

Meng,W., Lv, Z., Feng,M.,Zhang,S.,Li,M.,Mai,F.,2011. The origin of authigenic illite in tight sandstones and its effect on the formation of relatively high-quality reservoirs: A case study on sandstones in the 4th member of Xujiahe Formation, western Sichuan Basin. ACTA PETROLEI SINICA.32(5), 783-790.

Meng, W., Lv, Z., Liu, J., Tian, J., Feng, M., Li M., 2013. Resrvoir controlling factors and geological prediction models of the 4th member of the Xujiahe Formation in Xiaoquan-Xinchang area, the western Sichuan basin. Oil .Gas .Geol. 34, 483-490(in Chinese with English Abstract).

Morad, S., Al-Aasm, I.S., Nader, F.H., Ceriani, A., Gasparrini, M., Mansurbeg, H., 2012.Impact of diagenesis on the spatial and temporal distribution of reservoir quality in the Jurassic Arab D and C members, Offshore Abu Dhabi Oilfield, United Arab Emirates. GeoArabia17, 17-56.

Morad, S., Ketzer, J.M. De Ros, L.F., 2000. Spatial and temporal distribution of diagenetic alterations in siliciclastic rocks: implications for mass transfer in sedimentary basins. Sedimentology. 47 (Millenium Reviews), 95–120.

Ni, Y., Dai, J., Tao, S., Wu, X., Liao, F., Wu, W., Zhang, D., 2014. Helium signatures of gases from the Sichuan Basin, China. Org Geochem. 74, 33-43.

Shen, Z., Gong, Y., Liu S., Lv Z., 2010. A discussion on genesis of the upper Triassic Xujiahe Formation water in Xinchang area, Western Sichuan depression. Geological Review. 56(01):82-88(in Chinese with English Abstract).

Shi, L., 2010. Research on reservoir characteristics of the second member of the Upper Triassic Xujiahe Formation in Xiaoquan-Xinchang area,Western Sichuan Depression (master thesis) Yangtze university, Wuhan, Hubei, China.27-31 (in Chinese with English Abstract).

Surdam, R.C., Crossey, L.J., Hagen, E.S. & Heasler, H.P.,1989. Organic–inorganic interactions and sandstone diagenesis. AAPG Bull.73, 1–23.

Tang, J., Huang, Y., Xu, X., John, T., James, H., 2009. Application of converted-wave 3D/3-C data for fracture detection in a deep tight-gas reservoir. The leading edge.July, 826-837.

Tao, S., Zou, C., Mi, J.,Gao, X., Yang, C., Zhang, X., Fan, J., 2014. Geochemical comparison between gas in fluid inclusions and gas produced from the Upper Triassic Xujiahe Formation, Sichuan Basin, SW China. Org.Geochem. 74, 59-65.

Van der Plas, L., and A. C. Tobi, 1965, A chart for judging the reliability of point counting results. American Journal of Science. 263(1), 87–90, doi:10.2475/ajs.263.1.87.

Wang, J., 2012.The water-rock interaction mechanism of the relatively higher quality sandstone reservoirs formation in the fourth member of Xujiahe formation, Xiaoquan-FengGu area(master thesis). Chengdu University of Technology, Chengdu, Sichuan, China (in Chinese with English Abstract).

Wei, W., Zhu, X., Tan, M., Xue, M., Guo, D., Su, H., Wang, P., 2015. Diagenetic and porosity evolution of conglomerate sandstones in Bayingebi Formation of the Lower Cretaceous, Chagan Sag, China -Mongolia frontier area. Mar. Petrol. Geol. 66,998-1012.

Worden, R.H., Morad, S., 2000. Quartz cementation in oil field sandstones: a review of the key controversies. In: Worden, R.H., Morad, S. (Eds.), Quartz Cementation in Sandstonesstones. Wiley-Blackwell, pp. 1-20.

Worden, R.H., Morad, S., 2003. Clay minerals in sandstones: controls on formation, distributionand evolution. In: Warden, R.H., Morad, S. (Eds.), Clay mineral cements in sandstones International Association of Sedimentologists (IAS) Special Publication34. Blackwell, UK, pp. 3–41.

Xu C., Gehenn J M.,Zhao D.,Xie G.,Teng M K.,2015. The fluvial and lacustrine sedimentary systems and stratigraphic correlation in the Upper Triassic Xujiahe Formation in Sichuan Basin, China. AAPG Bull. 99, 2023–2041.

Ye, T., Zhang, H., Tang, J., 2009. Identification of high efficiency payzones with high permeability in deep fractured tight detrital reservoirs: A case study of gas reservoir in the Upper Triassic Xujiahe Formation of Xinchang gas field in western Sichuan basin. Nat. Gas Industry .29, 22-26.

Yuan, G., Cao, Y., Yang, T., Wang, Y., Li, X., Xi, K., Jia, Z., 2013.Porosity enhancement potential

through mineral dissolution by organic acids in the diagenetic process of clastic reservoir. Earth Science Frontier. 20(5), 207-219 (in Chinese with English Abstract).

Yuan, G., Gluyas, J., Cao, Y., Oxtoby, H.N., Jia, Z., Wang, Y., 2015a. Diagenesis and reservoir quality evolution of the Eocene sandstones in the northern Dongying Sag, Bohai Bay Basin, East China. Mar.Petrol. Geol. 22, 77–89.

Yuan, G., Cao, Y., Gluyas, J., Li, X., Xi, K., Wang, Y., Jia, Z., Sun, P., Oxtoby, N. H., 2015b.Feldspar dissolution, authigenic clays, and quartz cements in open and closed sandstone geochemical systems during diagenesis: Typical examples from two sags in Bohai Bay Basin, East China. AAPG Bull.99, 2121-2154.

Yuan, G., Cao, Y., Zhang, Y., Gluyas, J., 2017a. Diagenesis and reservoir quality of sandstones with ancient “deep” incursion of meteoric freshwater --An example in the Nanpu Sag, Bohai Bay Basin, East China. Mar.Petrol.Geol. 82, 444–464.

Yuan, G., Cao. Y., Qiu, L., Chen, C.,2017b. Genetic mechanism of highquality reservoirs in Permian tight fan delta conglomerates at the northwestern margin of the Junggar Basin, northwestern China: AAPG Bulletin.v.101, P. 1995-2019.

Zeng, J., Zhu, Z., Wu, Q., Peng, J., 2007. Experimental study on the generation of organic acids from source rocks and its effect factors. Acta Sedimentol. Sin. 25(6), 847-851(in Chinese with English abstract).

Zeng, L., 2010. Microfracturing in the UpperTriassic Sichuan Basin tight-gas sandstones:Tectonic, overpressure, and diagenetic origins. AAPG Bull.94, 1811-1825.

Zhang, G., 2005. Characteristics of fractures in the tight sandstone reservoirs of Xujiahe Formation in west Sichuan depression. Nat. Gas Industry. 25(7), 11-13.(in Chinese with English abstract).

Zhang J., Chang X., Wang S., 2002. Gas trap in deep basin of the upper Triassic in Sichuan Basin. Acta. Petrol.Sin.23, 27-33.

Zhang, X., 2011. The mechanism of feidspar dissolution and conservation in Upper Triassic Xujiahe Formation in Xinchang of Western Sichuan. (master thesis) Chengdu university of Technology for Master Degree, Chengdu, Sichuan, China.35-50(in Chinese with English Abstract).

Zheng,J., Ying,F.,1997. Reservoir Characteristics and Diagenetic model of sandstone intercalated in Coal-Bearing Strata. ACTA PETROLEI SINICA.18(4), 19-24.

Zheng R., Peng J., Gao H., Ke G., 2003. Analysis of the fracture active stages,heat fluid nature and the process of Forming reservoir in western Sichuan sag. J. Chengdu University Technology (Science and Technology Edition). 30,551-558 (in Chinese with English Abstract).

Table 1. Petrological composition of the T_3x^2 and T_3x^4 sandstones in the studied area

Stratum	Quartz, %	Feldspar, %	Rock fragment, %				Carbonate cement, %		Quartz cement, %
			Sedimentary rock, %	metamorphic rock, %	Volcanic rock, %	Total, %	Calcite	Dolomite	
T_3x^4	25.0-70.0 57.1	0.5–4.0 2.1	29.1	8.4	3.3	25.0-75.0 40.8	4.97	0.95	0.94
T_3x^2	63.3–80.0 70.0	3.0–13.0 8.3	10.0	10.0	1.7	17.0-30.0 21.7	3.72	2.96	2.16

Minimum-Maximum
Average

Table 2. Mineral contents in the T_3x^2 sandstones (XRD)

Well	Strata	Depth（m）	Whole rock(%)							Clay mineral(%)					
			Clay	Quartz	K-feldspar	plagioclase	Calcite	Dolomite	Illite	I/S	C/S	S/I	Smectite	Kaolinite	Chlorite
X11	T_3x^2	4755.72	4.8	85.2	0	8.4	0.6	0	85	0	0	0	0	0	15
X11	T_3x^2	4756.84	12.5	70.3	0	13.2	0	0.4	82	0	0	0	0	0	18
X11	T_3x^2	4757.77	8	73.9	0	16.9	0	1.2	74	0	0	0	0	0	26
X11	T_3x^2	4759.93	7.8	77.4	0	12.2	0	1	75	0	0	0	0	0	25
X11	T_3x^2	4762.66	4.4	83.7	0	11.5	0	0.4	67	0	0	0	0	0	33
X11	T_3x^2	4764.82	0.9	90.3	0	8.8	0	0	77	0	0	0	0	0	23
X11	T_3x^2	4766.62	0.01	90.3	0	9.7	0	0	73	0	0	0	0	0	27
X11	T_3x^2	4768.30	3.4	88.4	0	7.5	0	0.7	73	0	0	0	0	0	27
X10	T_3x^2	4847.63	6.4	92.1	0	0	0.4	1.1	67	0	0	0	0	0	33
X10	T_3x^2	4850.16	5.3	68.4	4.5	21.4	0	0.4	70	0	0	0	0	0	30
X10	T_3x^2	4851.34	7.1	80.2	3.4	8.3	0	1	71	0	0	0	0	0	29
X10	T_3x^2	4853.56	9.7	74.2	0	13.4	0	2.7	73	0	0	0	0	0	27
X10	T_3x^2	4855.15	2.3	80.8	3.5	10.4	0	3	73	0	0	0	0	0	27
X10	T_3x^2	4880.24	0.01	96.7	2	1.3	0	0	17	34	0	0	0	0	49
X10	T_3x^2	4924.32	2.7	73.7	8	15.4	0	0.2	24	0	0	0	0	0	76
X10	T_3x^2	4927.08	3.1	69.7	11.8	15.4	0	0	21	0	0	0	0	0	79
X10	T_3x^2	4927.83	2.7	70.1	13.3	13.6	0	0.3	24	0	0	0	0	0	76
X10	T_3x^2	4929.74	5	71.2	10.8	12.8	0	0.2	11	0	0	0	0	0	89
X10	T_3x^2	4930.19	2.3	76.3	14.1	7.2	0	0.1	20	0	0	0	0	0	80
X10	T_3x^2	4932.65	3	75.3	10.3	11.2	0	0.2	27	7	0	0	0	0	66
X10	T_3x^2	4936.12	3.9	75.4	9.3	11.4	0	0	23	0	0	0	0	0	77
X10	T_3x^2	4937.00	1.8	75.9	7.9	14.1	0.1	0.2	21	0	0	0	0	0	79
X11	T_3x^2	5018.02	7.5	68.6	10.1	13.6	0	0.2	26	0	0	0	0	0	74
X11	T_3x^2	5020.30	8.6	72	8.1	11.3	0	0	24	0	0	0	0	0	76
X11	T_3x^2	5021.53	9.6	67.7	6.5	15.5	0.3	0.4	27	0	0	0	0	0	73
X11	T_3x^2	5022.52	5.8	80.6	2.5	10.3	0.4	0.4	25	0	0	0	0	0	75
X11	T_3x^2	5064.68	6.3	78.2	8	7.1	0.1	0.3	36	0	0	0	0	0	64
X11	T_3x^2	5067.14	4.9	75	7.3	11.1	0.1	0	29	0	0	0	0	0	71
X11	T_3x^2	5070.01	4.4	76.1	10.5	8	0.8	0.2	43	0	0	0	0	0	57
X11	T_3x^2	5072.84	2.8	81	5	10.6	0.3	0.3	45	0	0	0	0	0	55
X11	T_3x^2	5075.64	1.3	76.5	6.6	15.3	0.3	0	48	0	0	0	0	0	52
X11	T_3x^2	5078.00	7.8	74.1	4.5	12.3	0.7	0.6	48	0	0	0	0	0	52
Average			4.9	77.8	5.3	11.3	0.2	0.5	46.8	1.3	0	0	0	0	51.9

Table 3. Mineral contents in the T_3x^4 sandstones (XRD)

Well	Strata	Depth（m）	Whole rock (%)						Clay mineral (%)						
			Clay mineral	Quartz	K-feldspar	plagioclase	Calcite	Dolomite	Illite	I/S	C/S	S/I	Smectite	Kaolinite	Chlorite
X11	T_3x^4	3466.57	4.5	92.3	0	0	3.2	0	55	0	0	0	0	27	18
X11	T_3x^4	3468.31	4.9	94.3	0	0	0.7	0.1	49	0	0	0	0	26	25
X11	T_3x^4	3470.64	11.1	88.2	0	0	0.7	0	41	0	0	0	0	24	35
X11	T_3x^4	3472.00	11.3	88.3	0	0	0	0.4	44	0	0	0	0	17	39
X11	T_3x^4	3474.12	12.4	86.1	0	1	0.2	0.3	41	12	0	0	0	32	15
X11	T_3x^4	3475.67	1.6	96.5	0	0	1.9	0	58	0	0	0	0	0	42
X11	T_3x^4	3476.84	3.4	93.4	0	0.7	2.3	0.2	66	0	0	0	0	0	34
X11	T_3x^4	3478.90	7	91.9	0	0	0.8	0.3	58	0	0	0	0	16	26
X11	T_3x^4	3481.05	6	93.6	0	0	0.3	0.1	18	0	0	0	0	0	82
X11	T_3x^4	3481.66	16.1	83.4	0	0	0.3	0.2	55	0	0	0	0	0	45
X11	T_3x^4	3575.31	0	55.5	0	0	35.3	9.2	54	0	0	0	0	0	46
X11	T_3x^4	3579.55	0	61.6	0	0	26.3	12.1	73	0	0	0	0	0	27
CX568	T_3x^4	3402.10	6.8	89.3	0	0	1.8	2.1	63	0	0	0	0	22	15
CX568	T_3x^4	3403.45	1.5	96.7	0	0	1.3	0.5	39	0	0	0	0	50	11
CX568	T_3x^4	3404.10	7.3	90.6	0	0	1.4	0.7	31	10	0	0	0	39	20
CX568	T_3x^4	3405.03	6.4	90.3	0	0	1.7	1.6	44	0	0	0	0	40	16
CX568	T_3x^4	3406.22	9.7	88.6	0	0	0.9	0.8	22	20	0	0	0	43	15
CX568	T_3x^4	3406.77	7.1	89.6	0	0	2.4	0.9	37	5	0	0	0	39	19
CX568	T_3x^4	3408.59	5.1	92	0	0	2.2	0.7	28	18	0	0	0	35	19
CX568	T_3x^4	3410.71	6.5	92.5	0	0	0.6	0.4	53	0	0	0	0	25	22
CX568	T_3x^4	3412.35	2.2	96.8	0	0	0.5	0.5	51	0	0	0	0	37	12
CX568	T_3x^4	3414.23	5.9	93.1	0	0	0.6	0.4	52	0	0	0	0	36	12
CX568	T_3x^4	3422.85	6.1	90.1	0	0	3.5	0.3	39	0	0	0	0	30	31
CX568	T_3x^4	3424.87	5.1	93.3	0	0	0.8	0.8	53	0	0	0	0	27	20
CX568	T_3x^4	3426.10	7.3	90.8	0	0	1.5	0.4	36	0	0	0	0	16	48
CX568	T_3x^4	3428.36	2	67.5	0	0	19.3	11.2	53	0	0	0	0	0	47
CX568	T_3x^4	3469.00	5	79.7	0	0	11.9	3.4	43	0	0	0	0	32	25
CX568	T_3x^4	3481.10	6.8	43.2	0	0	26.5	23.5	22	0	0	0	0	72	6
CX568	T_3x^4	3546.66	10.2	84.9	0	0	2.8	2.1	26	0	0	0	0	57	17
CX568	T_3x^4	3713.17	7.5	80.5	0	0	9.7	2.3	27	0	0	0	0	58	15
CX568	T_3x^4	3714.05	4.6	83	0	0	10	2.4	31	0	0	0	0	54	15
CX568	T_3x^4	3715.00	3.8	90.7	0	0	4.5	1	17	6	0	0	0	55	22
CX568	T_3x^4	3721.37	0.20	47.5	0	0	40.3	12.2	41	8	0	0	0	30	21
	Average		5.9	84.7	0	0	6.6	2.8	43	2.4	0	0	0	28.5	26.1

Table 4 Electron probe characteristics of carbonate cement within the Xujiahe sandstones of Xinchang structural belt

Stratigraphy	Type of cement	Oxide content（%）			molar fraction（%）			Samples
		MgO	CaO	FeO	MgCO3	CaCO3	FeCO3	
The second member	Dolomite cement	8.87	29.76	12.60	25.67	62.60	20.86	10
The second member	Calcite cement	0.67	53.26	1.49	1.67	95.73	2.09	5
The fourth member	Calcite cement	0.23	54.00	1.05	0.57	97.74	1.48	25
	Total	2.44	47.85	3.99	6.98	88.70	6.40	40

Table 5. Types and isotopic features of carbonate cements and fragments n the T_3x^4 sandstone in Xinchang structural belt , Western Sichuan Basin.

Well	Depth（m）	Carbonate minerals	Types of occurrence	$\delta^{13}C_{PDB}$（‰）	$\delta^{18}O_{PDB}$（‰）
FG21	3516.74	Calcite cement	The primary pore	1.85	-10.06
CG561	3699.75	Calcite cement	The primary pore	0.24	-8.75
CF563	3744.21	Calcite cement	The primary pore	2.46	-5.51
FG21	3749.58	Calcite cement	The primary pore	1.07	-8.24
FG21	3764.75	Calcite cement	The primary pore	1.27	-6.86
FG21	3772.23	Calcite cement	The primary pore	2.15	-6.03
FG21	3776.7	Calcite cement	The primary pore	2.55	-4.75
CF563	3778.17	Calcite cement	The primary pore	2.31	-7.3
FG21	3778.7	Calcite cement	The primary pore	1.53	-6.41
FG23	3869.14	Calcite cement	The primary pore	-0.13	-9.92
XC22	3403.6	Calcite cement	The secondary pore	-2.85	-18.61
CX568	3404.1	Calcite cement	The secondary pore	-1.32	-13.61
CX568	3406.77	Calcite cement	The secondary pore	-1.2	-13.61
XC22	3412.08	Calcite cement	The secondary pore	-2.99	-17.89
CX568	3426.1	Calcite cement	The secondary pore	-0.76	-13.49
X11	3466.565	Calcite cement	The secondary pore	-3.47	-15.03
X11	3470.635	Calcite cement	The secondary pore	-2.93	-14.44
X11	3475.67	Calcite cement	The secondary pore	-3.61	-15.23
X11	3476.835	Calcite cement	The secondary pore	-2.31	-13.97
X11	3478.9	Calcite cement	The secondary pore	-3.19	-14.59
X11	3481.05	Calcite cement	The secondary pore	-2.44	-13.71
XC26	3481.81	Calcite cement	The secondary pore	-1.75	-17.4
XC26	3483.48	Calcite cement	The secondary pore	0.1	-10.77
XC26	3484.37	Calcite cement	The secondary pore	-0.08	-14.68
CF563	3511.77	Calcite cement	The secondary pore	-4.67	-19.71
CX560	3514.175	Calcite cement	The secondary pore	-1.46	-14.06
CX565	3547.62	Calcite cement	The secondary pore	-3.51	-15.29
CX565	3548.17	Calcite cement	The secondary pore	-2.99	-14.58
CX565	3549.33	Calcite cement	The secondary pore	-2.75	-14.65

CX565	3558.33	Calcite cement	The secondary pore	-2.97	-14.59
XC29	3628.47	Calcite cement	The secondary pore	-3.37	-13.71
XC29	3629.75	Calcite cement	The secondary pore	-3.31	-12.87
CX565	3642.44	Calcite cement	The secondary pore	-5.43	-16.55
XC27	3661.82	Calcite cement	The secondary pore	-4.63	-14.99
XC27	3661.82	Calcite cement	The secondary pore	-3.42	-12.64
CG561	3694	Calcite cement	The secondary pore	-5.18	-18.93
CF563	3873.93	Calcite cement	The secondary pore	0.75	-15.42
CG561	4007.19	Calcite cement	The secondary pore	-1.92	-13.24
CX568	3469	Calcite	Rock fragment	1.92	-7.1
CX568	3721.37	carbonate	Rock fragment	1.35	-9.74
FG21	3767.45	carbonate	Rock fragment	1.63	-4.81
XC27	4018.12	carbonate	Rock fragment	1.85	-7.75
CX568	3410.71	Dolomite cement	The secondary pore	-0.97	-13.32
CX568	3414.23	Dolomite cement	The secondary pore	-0.81	-12.91
CF563	3873.93	Dolomite cement	The secondary pore	1.97	-10.94
XC28	3685.68	Domlomite	Rock fragment	1.33	-9.23
CF563	3744.21	Domlomite	Rock fragment	2.11	-5.64
FG21	3767.45	Domlomite	Rock fragment	2.01	-5.56
FG21	3775.6	Domlomite	Rock fragment	1.53	-5.99
FG21	3775.6	Domlomite	Rock fragment	2.22	-4.87
FG21	3776.7	Domlomite	Rock fragment	2.13	-5.45
CX568	3428.36	Domlomite	Rock fragment	1.46	-8.44
CX568	3481.1	Domlomite	Rock fragment	1.89	-7.8
CX568	3546.66	Domlomite	Rock fragment	1.72	-7.6
X11	3579.55	Domlomite	Rock fragment	1.5	-6.78

Table 6.Types and isotopic features of carbonate cements and fragments, n the $T3x^2$ sandstone in Xinchang structural belt, Western Sichuan Basin.

Well	Depth（m）	Carbonate minerals	Types of occurrence	$\delta^{13}C_{PDB}$（‰）	$\delta^{18}O_{PDB}$（‰）	Temp(℃)
XC12	4819.45	Calcite cement	The residual primary pore and secondary pore	-0.06	-16.65	117.5
GM2	4992.3	Calcite cement	The residual primary pore and secondary pore	-1.33	-16.09	113.3
GM4	5114.97	Calcite cement	The residual primary pore and secondary pore	0.05	-12.64	88.2
XC8	5175.37	Calcite cement	The residual primary pore and secondary pore	-0.11	-12.47	87.1
XC7	5287.98	Calcite cement	The residual primary pore and secondary pore	0.99	-12.98	90.6
XC7	5291.33	Calcite cement	The residual primary pore and secondary pore	1.15	-13.45	93.9
X11	4755.72	Calcite cement	The residual primary pore and secondary pore	0.05	-12.56	87.7
CG561	4997.72	Calcite cement	The residual primary pore and secondary pore	1.7	-16.36	115.3
X11	5070.01	Calcite cement	The residual primary pore and secondary pore	-1.25	-16.64	117.5
X11	5075.64	Calcite cement	The residual primary pore and secondary pore	-0.33	-10.88	76.4
GM2	4711.55	Dolomite cement	The secondary pore	0.53	-12	83.9
XC8	5009.28	Dolomite cement	The secondary pore	2.18	-12.17	85.0
GM2	5118.96	Dolomite cement	The secondary pore	3.69	-9.77	69.2
DY1	5323.87	Dolomite cement	The secondary pore	1.86	-15.17	106.4
X11	4757.765	Dolomite cement	The secondary pore	0.42	-9.97	70.5
X10	4851.34	Dolomite cement	The secondary pore	-0.38	-12.87	89.8
X10	4853.56	Dolomite cement	The secondary pore	2.5	-12.76	89.1
X10	4855.15	Dolomite cement	The secondary pore	1.68	-13.55	94.6
GM4	4889.09	Dolomite cement	The secondary pore	-1.81	-12.77	89.1
X10	4924.32	Dolomite cement	The secondary pore	4.97	-13.83	96.6
X10	4927.83	Dolomite cement	The secondary pore	8.7	-9.56	67.9
X10	4932.65	Dolomite cement	The secondary pore	-0.04	-14.36	100.4
X10	4937	Dolomite cement	The secondary pore	2.44	-11.94	83.5
X11	5022.52	Dolomite cement	The secondary pore	1.45	-10.3	72.6
CX565	5058.73	Dolomite cement	The secondary pore	0.4	-13.06	91.2
X11	5078	Dolomite cement	The secondary pore	-0.52	-14.47	101.2
DY1	5427.4	Dolomite cement	The secondary pore	2.58	-16.65	117.5
XC12	4812.34	Domlomite	Rock fragment	6.16	-8.79	
X10	4847.63	Domlomite	Rock fragment	1.25	-3.62	
CX565	5062.08	Domlomite	Rock fragment	1.01	-8.87	

Figure captions

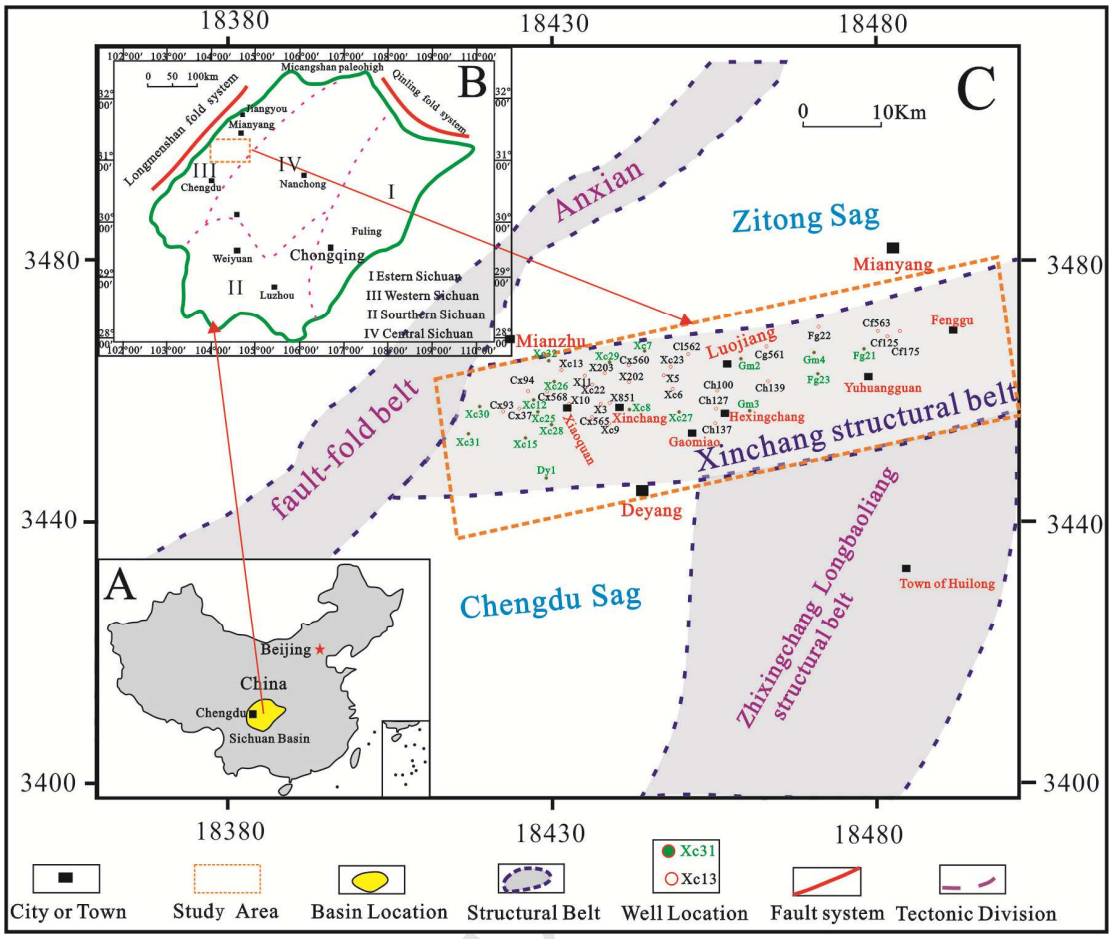

Fig. 1. The geographical and structural map showing the location of the study area which mainly comprises of the Xinchang structural belt. (A) Location map showing the location of Sichuan basin in China. (B) The tectonic feature of Sichuan basin indicates that the Western Sichuan basin foreland belong to the Western Sichuan depression. (C) Structural map of the Western Sichuan foreland basin showing the location of the Xinchang structural belt. Green wells represent key wells with hydrocarbon show.

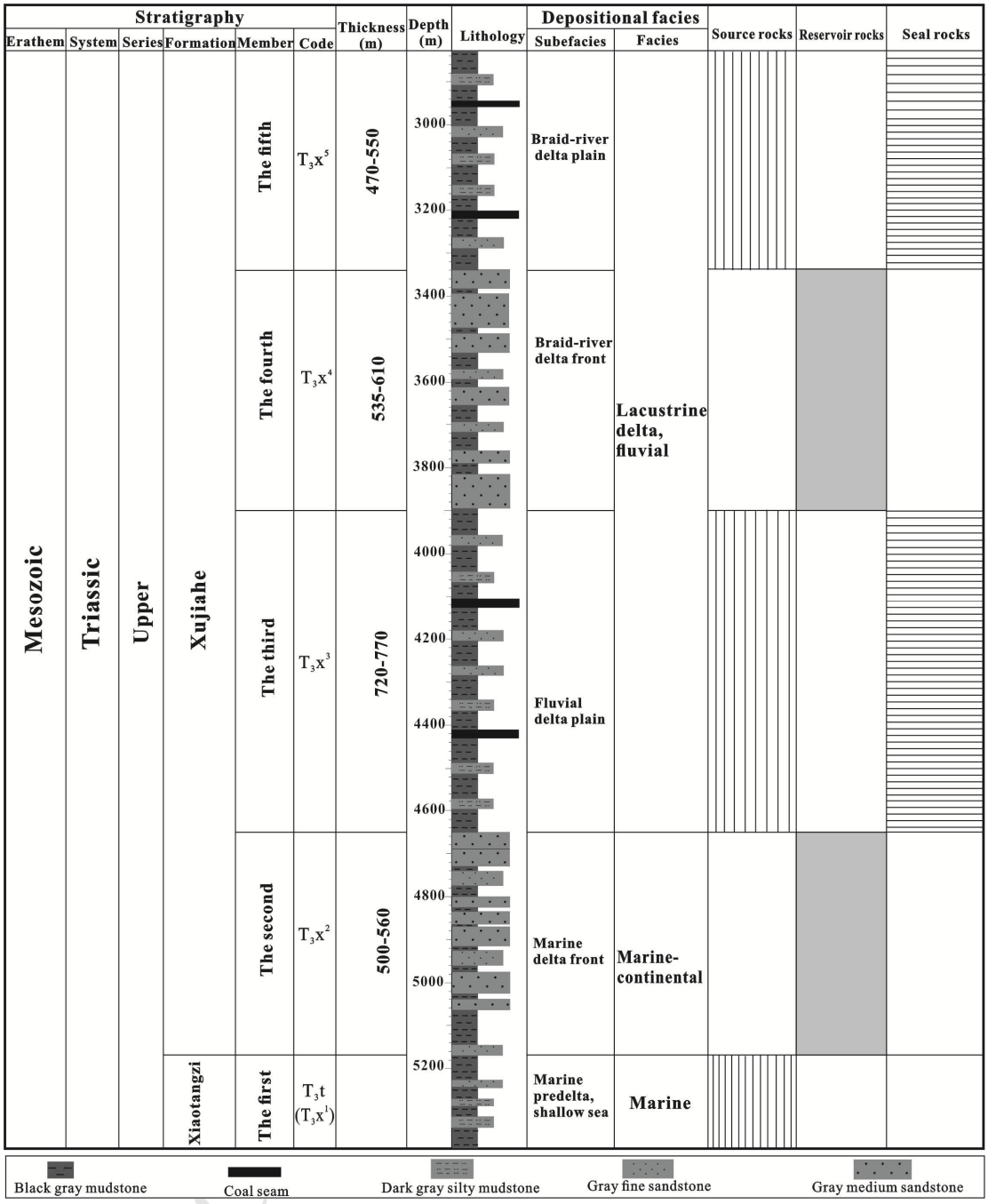

Fig. 2. Stratigraphic column of the Western Sichuan depression showing that the Xujiahe Formation sandstones. Abbreviations: T_3x^2 = The second member of the Xujiahe Formation; T_3x^3 = The third member of the Xujiahe Formation; T_3x^4 =The fourth member of the Xujiahe Formation; T_3x^5 =The fifth member of the Xujiahe Formation. T_3x^1 = The Xiaotangzi and Maantang Formations,

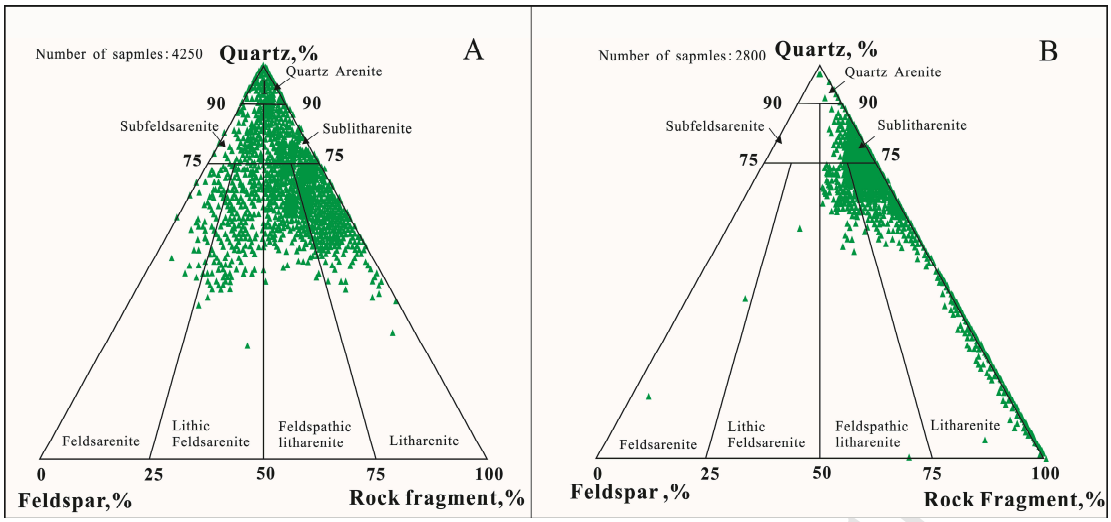

Fig. 3. Ternary plots showing grain composition of sandstones from T_3x^2 sandstone (A) and T_3x^4 sandstone (B) (refer to sandstone classification standard of Folk et al., 1980)

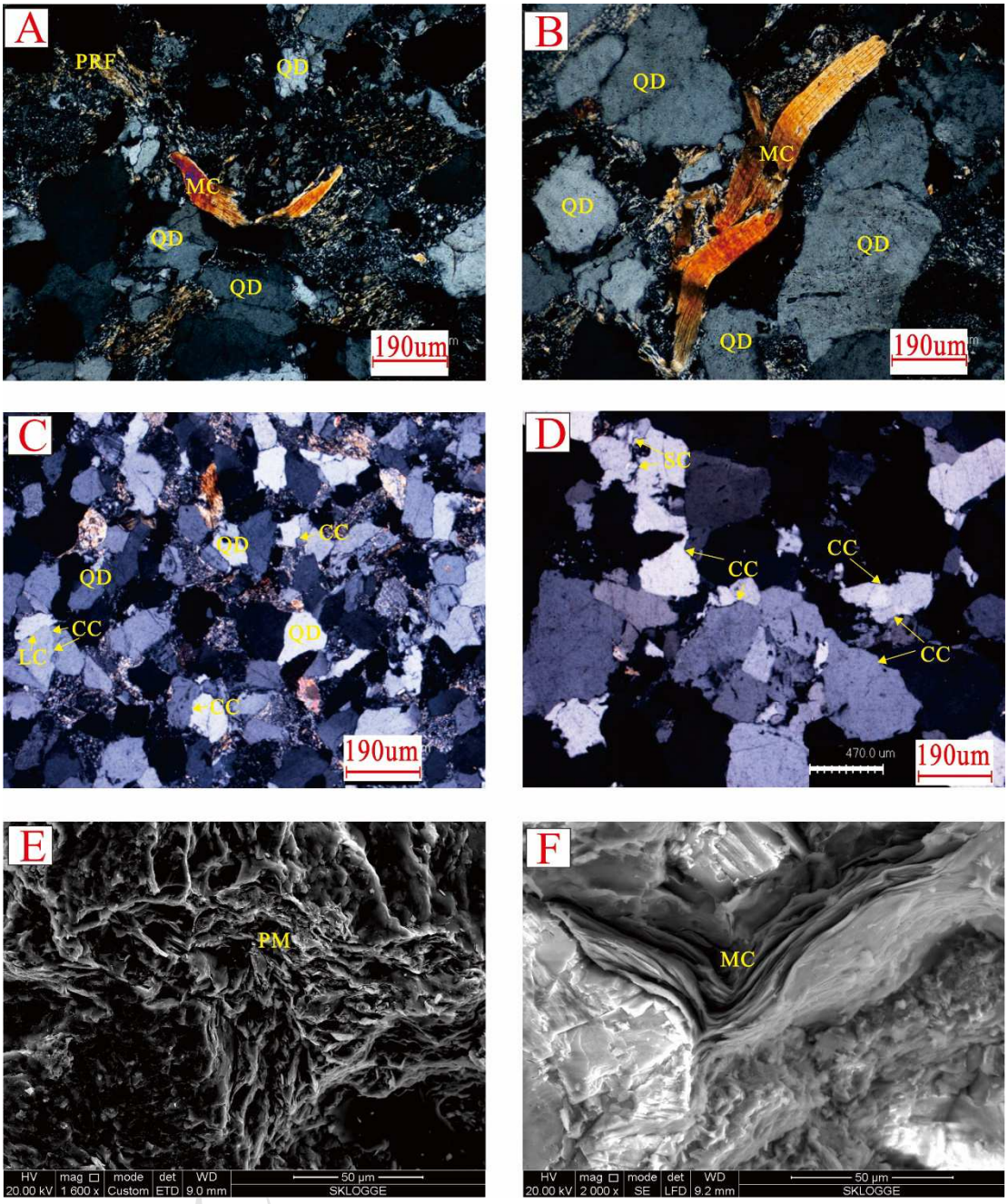

Fig. 4. The compaction characteristics in the T_3x^2 and T_3x^4 sandstones.(A) Optical photomicrographs of thin section (XPL) showing the deformation of mica (MC) and plastic rock fragments (PRF), pseudomatrix from mud intraclasts. Well XC27, 3589.91m, $T3X^4$. (B) Optical photomicrographs of thin section (XPL) showing the deformation of mica (MC).well DY1,4197.63m, T_3x^4.(C) Optical photomicrographs of thin section (XPL) showing the long (LC) and concave–convex contacts(CC) between quartz–quartz grains. Well XC15, 4950.7m, T_3x^2. (D) Optical

photomicrographs of thin section (XPL) showing the concave–convex (CC) and sutured contacts (SC) between quartz–quartz grain. wellXC12, 4828.44m, T_3x^2. (E) SEM image showing the pseudomatrix formed by the deformation of plastic rock fragments. well DY1,5320.05m, T_3x^2.(F) SEM image showing the deformation of mica (MC).well XC31,3741.77m, T_3x^4.

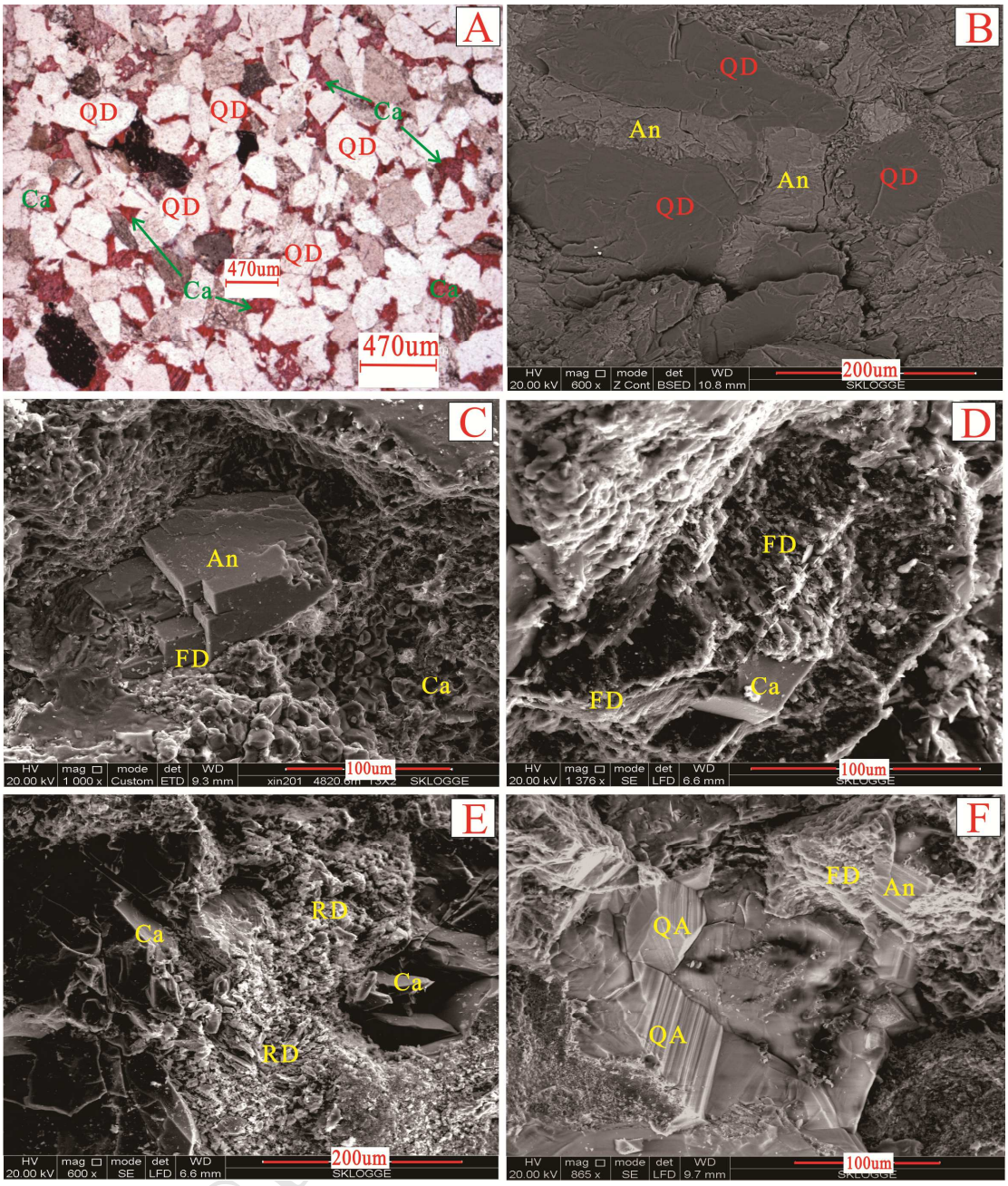

Fig. 5. The carbonate cement characteristics in the T_3x^2: (A) Optical photomicrograph (PPL) showing the calcite (Ca) filling in the intergranular pores, QD-detrital quartz, Well GM2,4722.33m,T_3x^2 (B) BSE image showing dolomite (ankerite) cement (An) filling the intergranular pores, well GM2, 4822.0m, T_3x^2. (C) SEM image showing the euhedral dolomite(ankerite) (An) filling the intragranular dissolved pores, well X201, 4820.6m, T_3x^2. (D) SEM image showing calcite(Ca) replacing the feldspar with the dissolution(FD),well GM4,4887.85m, T_3x^2.(E) SEM image showing calcite

replacing the rock fragments companying with the dissolution(RD), GM4,4887.85m, T_3x^2.(F) SEM image showing authigenic dolomite(ankerite) (An) and quartz(QA) replacing feldspar and filling the dissolved pore of feldspar, which suggest calcite and quartz cement are related with the feldspar dissolution(FD). well GM3,4922.21m, T_3x^2.

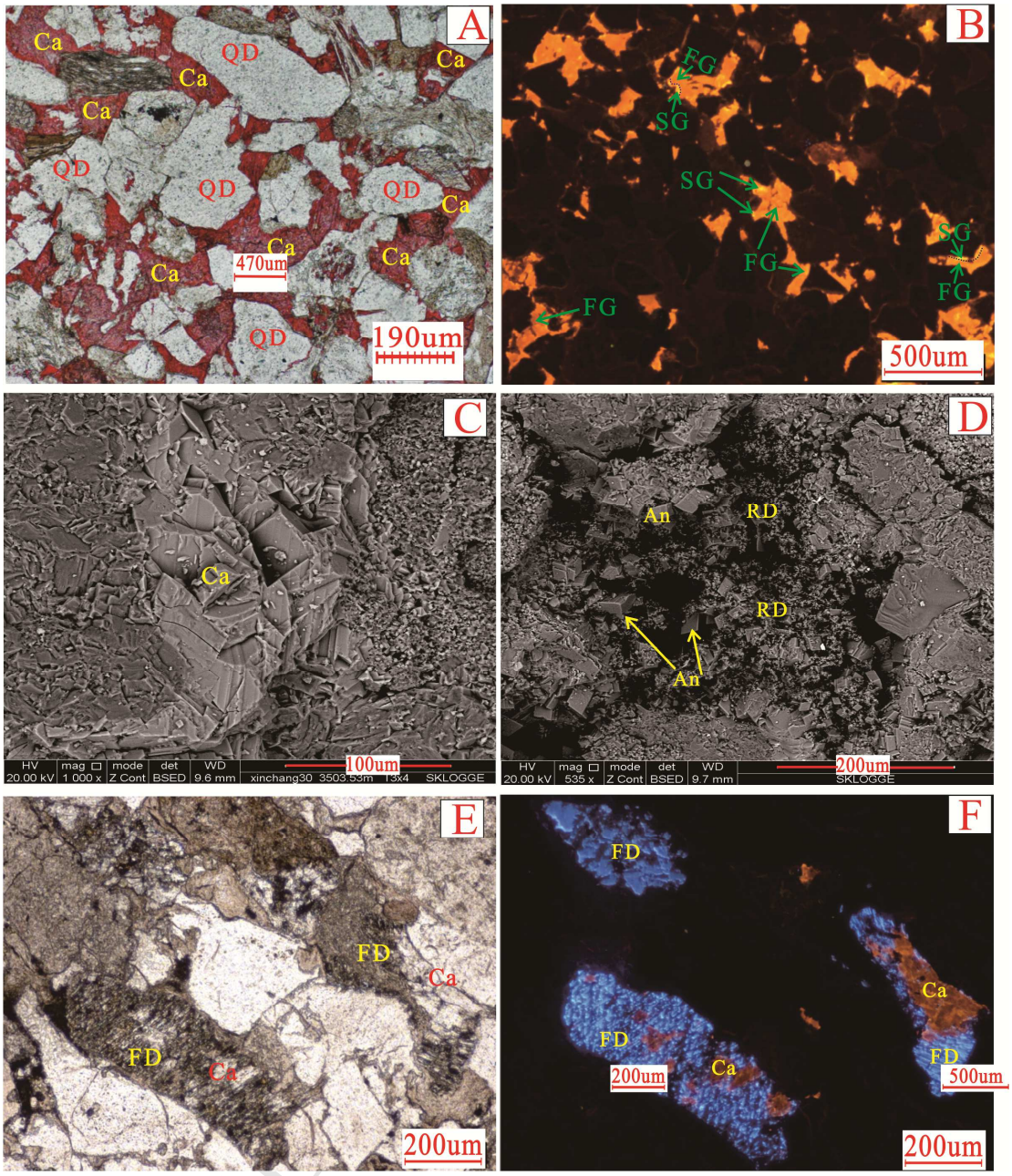

Fig. 6. The carbonate cement characteristics in the T_3x^4 sandstones: (A) Optical photomicrograph (PPL) showing basal calcite cement (Ca) filling the intergranular pores, well XC15, 3636.57m, T_3x^4. (B) Cathodoluminoscope image showing two generation of calcite: saffron yellow micro-crystal calcites filling the primary pores represent the first generation (FG), the orange red calcite cements filling residual primary pore and secondary pores as partially replacement of some detrital grains, represent the second generation (SG).well X5, 3673.43m, T_3x^4. (C) BSE image

showing calcite (Ca) filling in the intergranular pores, well XC30,3503.53m, T_3x^4. (D) BSE image showing authigenic euhedral dolomite (ankerite) (An) filling in the intergranular dissolved pores that formed by dissolution of carbonate rock fragments, well FG21, 3758.6m, T_3x^4.(E) Optical photomicrograph (PPL) showing calcite(Ca) replacing the feldspar with the dissolution(FD), well X5,3598.59m,T_3x^4.(F). Cathodoluminoscope image responding to the (E) shows the saffron yellow calcite cements (Ca) replacing the blue feldspar, and the intragranular dissolved pores caused by the feldspar dissolution (FD). well X5,3598.59m,T_3x^4.

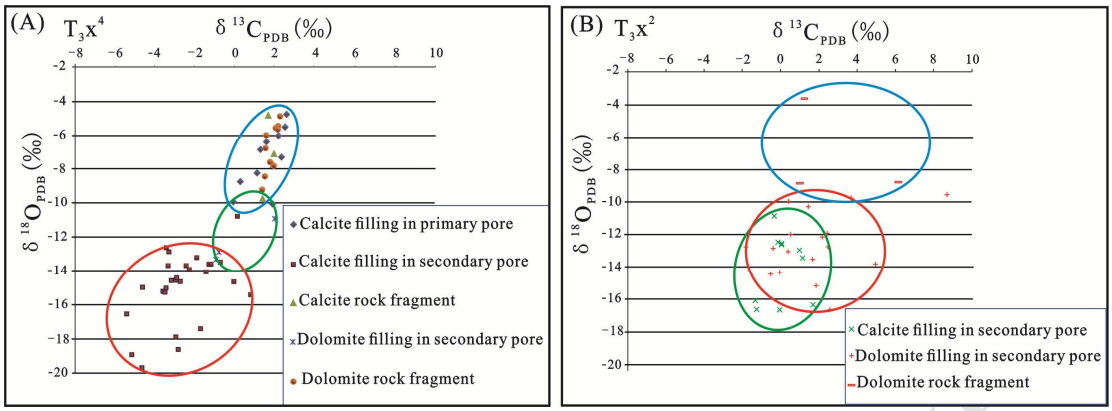

Fig. 7. The $\delta^{18}O$-$\delta^{13}C$ diagram of various carbonate cement within the sandstones of the T_3x^4 (A) and T_3x^2 (B) of the Xujiahe Formation.

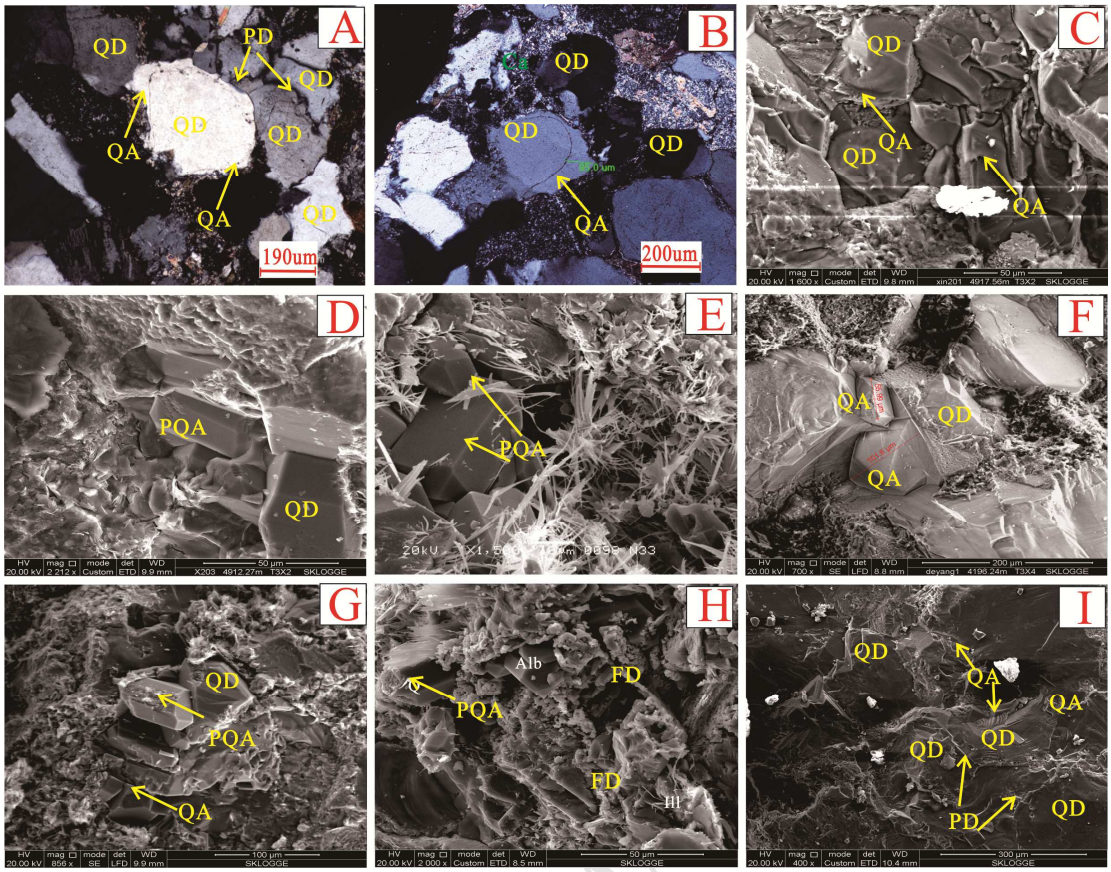

Fig. 8. The quartz cement characteristics in the T_3x^2 and T_3x^4 sandstones.(A) The optical photomicrograph of thin section (PPL) showing quartz overgrowth(QA),which occur near the pressure dissolution(PD),QD- detrital quartz. well DY1,5341m, T_3x^2 . (B) The optical photomicrograph of thin section (PPL) showing quartz overgrowth (QA), QD-detrital quartz. well XC25,3775.25m, T_3x^4. (C) SEM image showing quartz overgrowth (QA), QD- detrital quartz. Well X201,4917m, T_3x^2.(D) SEM image showing isolated pore-filling authigenic quartz crystal (PQA).,well X203,4912.27m, T_3x^2.(E) SEM image showing the isolated authigenic quartz crystals (PQA) and illite(I) filling the intergranular pores,well CX568,3412.35m, T_3x^4. (F) SEM image showing the quartz overgrowth(QA),well DY1,4196.24m, T_3x^4.(G) SEM image showing the authigenic quartz including the isolated pore-filling quartz crystal(PQA) and quartz overgrowth(QA), both of which were partly replaced by the illite(I).well GM3,3780.2m T_3x^4.(H) SEM image

showing the isolated pore-filling authigenic quartz (PQA),albite(Alb) and illite(I) filling in the dissolved pores which were formed by the feldspar dissolution(FD). Well X201,4917.0m, T_3x^2.(I) SEM image showing the quartz overgrowth(QA) occur together with the pressure dissolution(PD).well GM2,4736m, T_3x^2.

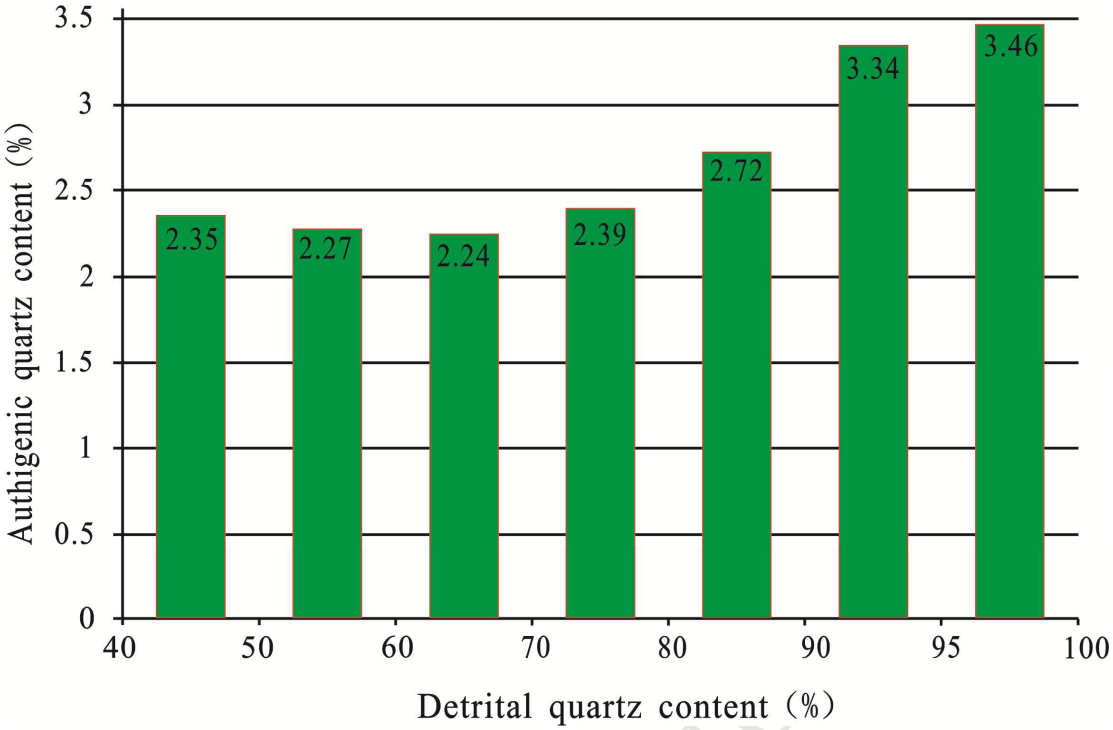

Fig. 9. The average content relationship between the detrital quartz and the authigenic quartz cements.

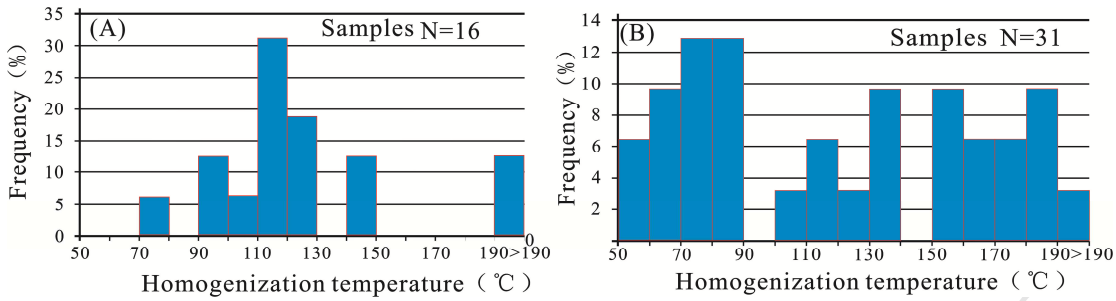

Fig. 10. Frequency histogram of homogenization temperature from inclusions in authigenic quartz cements in the T_3x^4 (A) and T_3x^2 (B) (Luo et al., 2015).

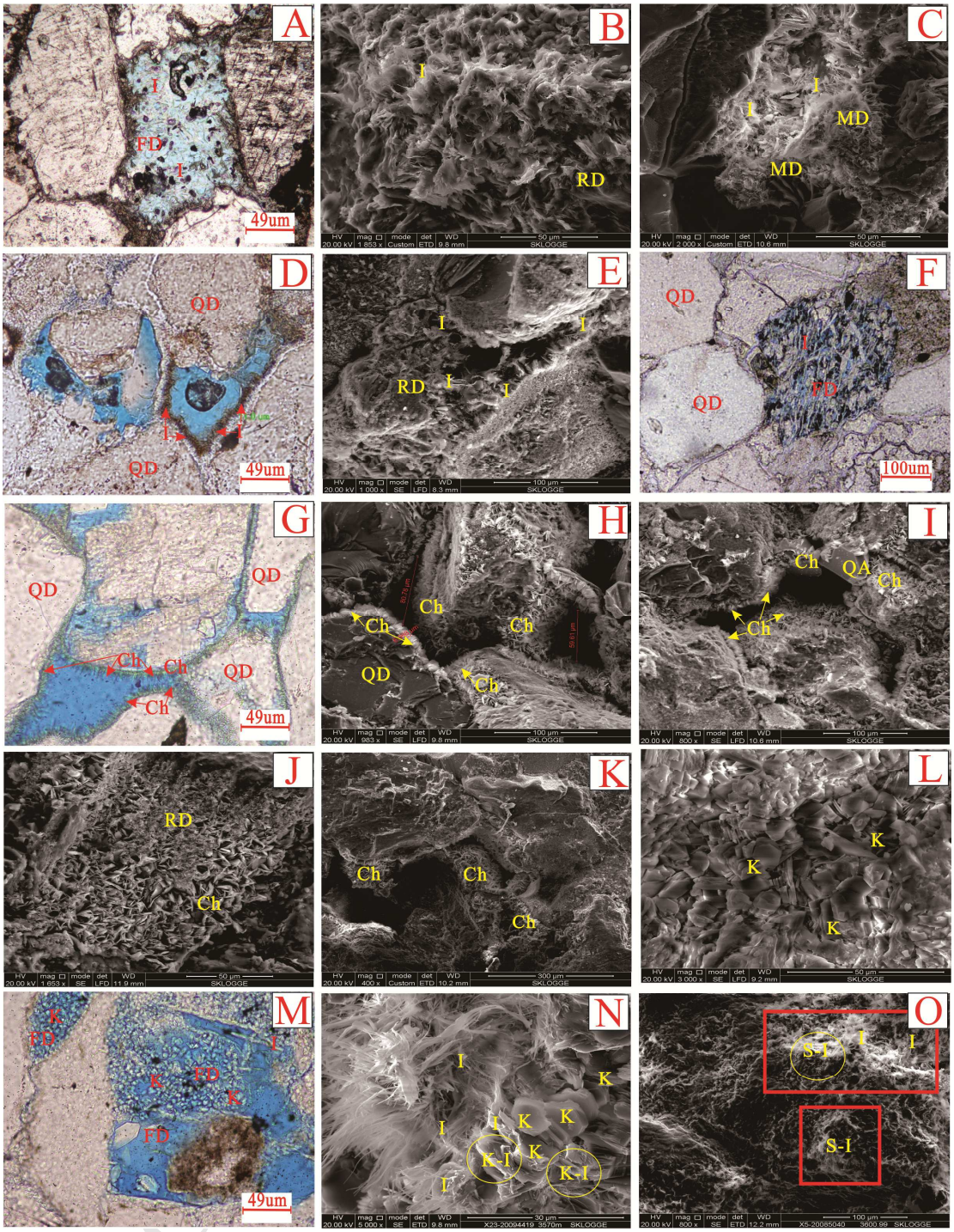

Fig. 11. The clay minerals characteristics in the T_3x^2 and T_3x^4 sandstones.(A) The optical photomicrograph of thin section (PPL) showing authigenic illite (I) occurring as netted aggregates filled in intragranular dissolved pores., which is related with the feldspar dissolution(FD). well X10,4884.53m, T_3x^2.(B) SEM image showing illite(I) replaced the rock fragments,which is related with rock fragments

dissolution(RD).well GM2,4714.69m, T_3x^2. (C) SEM image showing non-netted aggregates illite related with the illitization of matix. well GM2,4714.69m, T_3x^2. (D) The optical photomicrograph of thin section (PPL) showing authigenic illite(I) occurring as grain-coatings. well XC27,3670.64m, T_3x^4.(E) SEM image showing the filamentous(netted aggregates) illite filling in the dissolved pore of rock fragments.3787.4m. T_3x^4. (F) The optical photomicrograph (PPL) showing authigenic illite occurring as netted aggregates filled in intragranular dissolved pores of feldspar.well X5,3673.47m, T_3x^4.(G) The optical photomicrograph (PPL) showing the the chlorite rim(Ch) occurring as grain-coating. well CG561,4992.9m, T_3x^2.(H) SEM image showing the chlorite rim(Ch) as the grain-coating.well DY1,5530.86m, T_3x^2. (I)SEM image showing the chlorite rim(Ch) as the grain-coating accompanied by authigenetic quartz (QA) filling intergranular pores well GM2,5038.9m, T_3x^2. (J) SEM image showing chlorite (Ch) filling in the dissolved pore formed by the rock volcanic fragments dissolution (RD).well GM2,4994.06m, T_3x^2 . (K) SEM image showing the pore-filling chlorite. well GM4, 3786.11m, T_3x^2. (L) SEM image showing pseudohexagonal kaolinite occurring as vermicular or booklet-like aggregates. well FG21,3755.49m, T_3x^4.(M) The optical photomicrograph (PPL) showing kaolinite(K) formed by the feldspar dissolution(FD). Well CX565,3549.53m, T_3x^4.(N) SEM image showing booklet-like pseudohexagonal kaolinite(K) which partly transformed into the filamentous illite(I).well XC23,3570m, T_3x^4.(O) SEM image shows the flaky smectite transforming into filamentous illite(I) ,(S-I)-mixed layer I/S. well X5,3600.99m, T_3x^4.

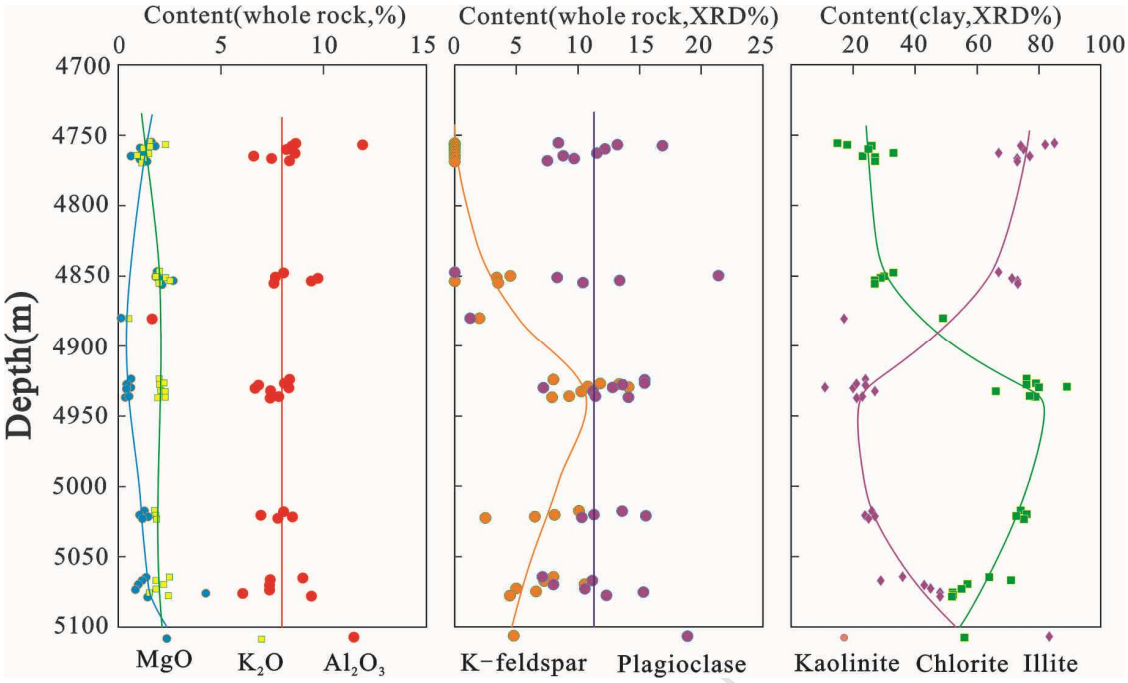

Fig. 12. Vertical variation of the content of typical major elements, feldspar and clay minerals in the T_3x^2 sandstones. The content of kaolinite, chlorite and illite represent relative content in clay minerals.

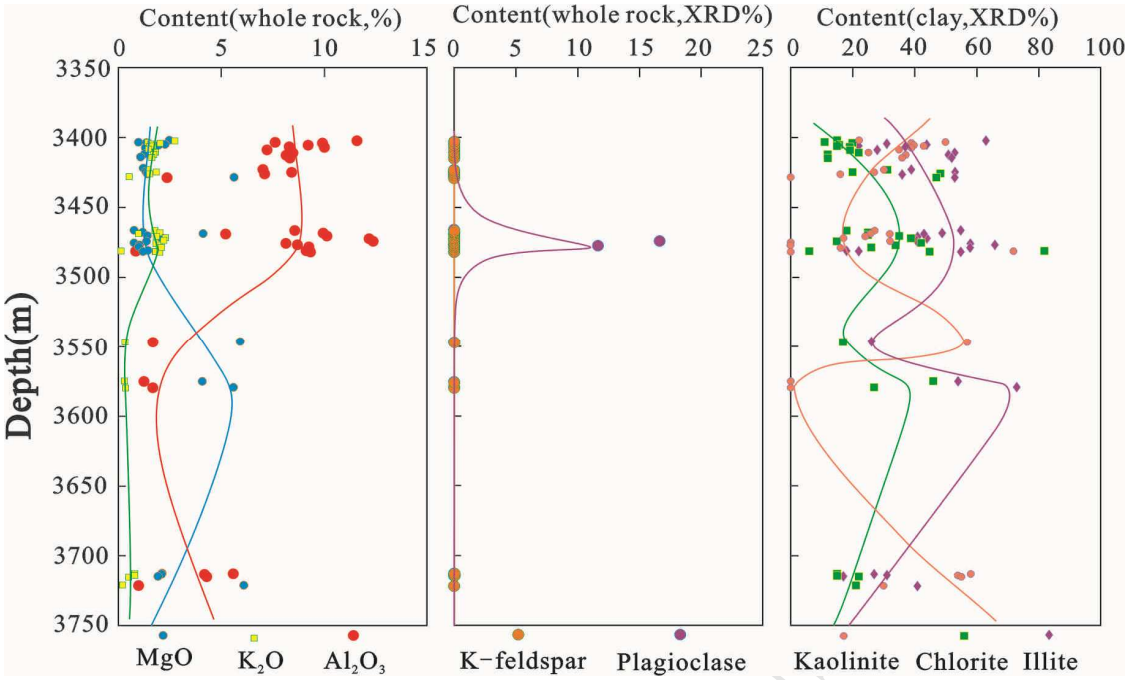

Fig. 13. Vertical variation of the content of typical major elements, feldspar and clay minerals in the T_3x^4 sandstones. The content of kaolinite, chlorite and illite represent relative content in clay minerals.

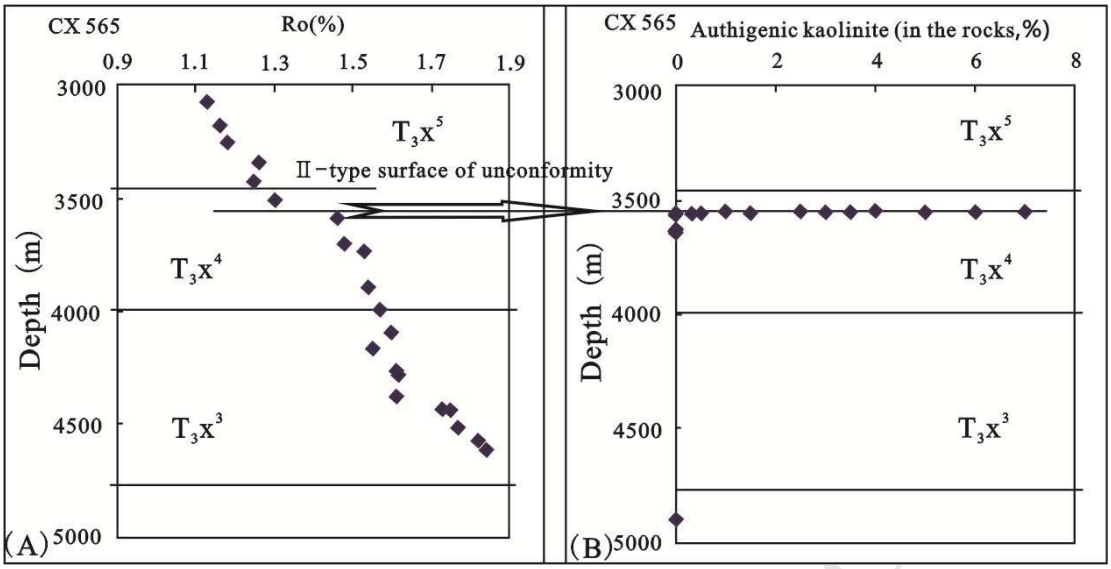

Fig. 14. The scatter diagram of Ro –depth and kaolinite-depth in the Xujiahe Formation of well CX565 (Based on Zhang, 2011). (a) The Ro –depth scatter diagram of the well CX565 show an outlier of the Ro exist in the top of the T_3x^4. (a) and (b) indicate that the depth of outlier of Ro corresponds to the developmental zone of kaolinite.

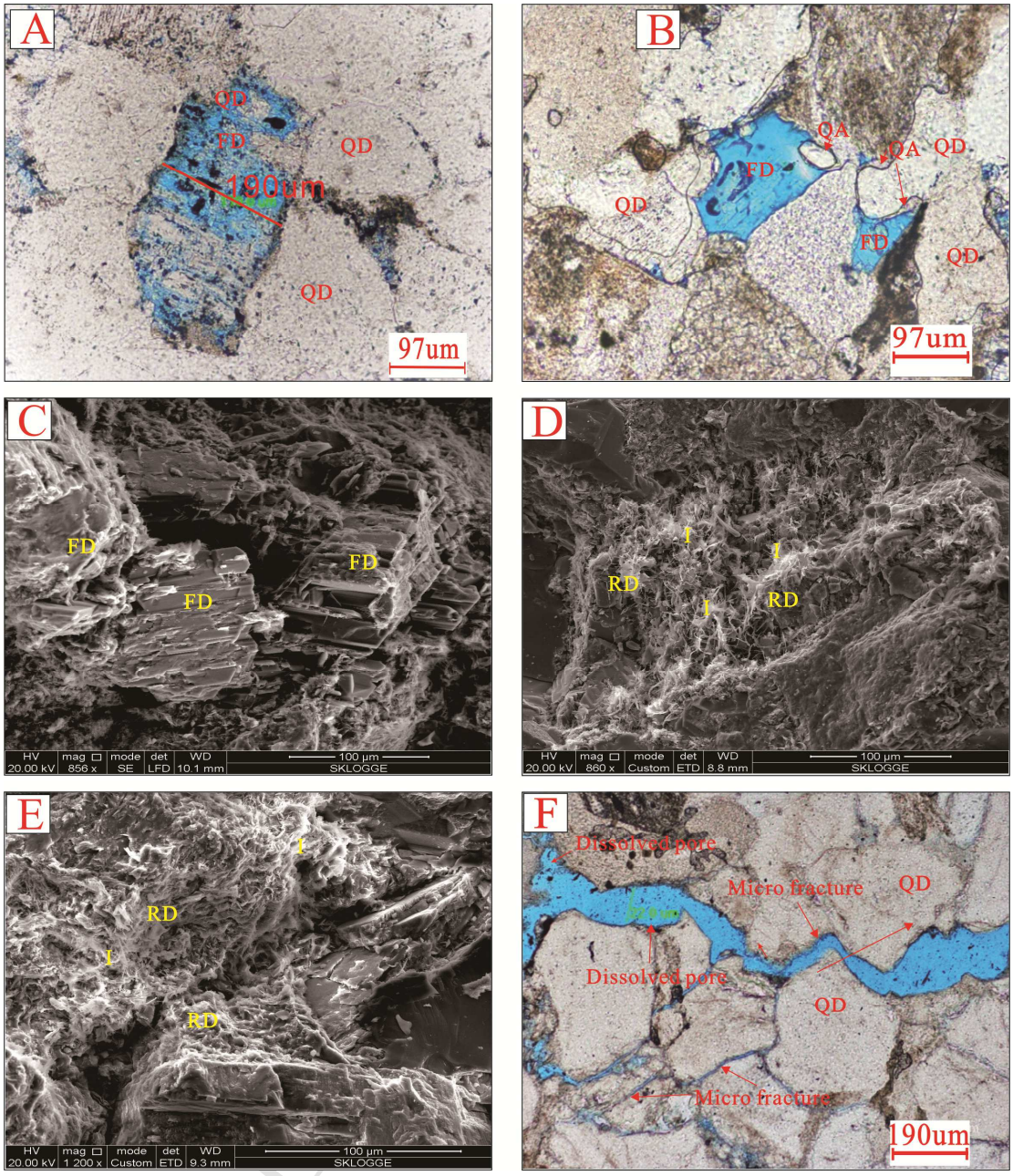

Fig. 15. The dissolution characteristics of feldspar and rock fragments in the T3X2 and T_3x^4 sandstones. (A) Optical photomicrographs of thin section(PPL) showing the feldspar partly dissolved.well GM4,3788.92m, T_3x^4.(B) Optical photomicrographs of thin section(PPL) showing the feldspar completely dissolved.well xc15,3625.28m, T_3x^4.(C) SEM image showing feldspar partly dissolved. well GM3,4079.48m, T_3x^4.(D) SEM image showing the illite (I) companying the rock fragment dissolution (FD).well GM4,4888.77m, T_3x^2.(E))

SEM image showing the illite (I) companying the rock fragment dissolution (FD).well gm4,4087.11m, T_3x^4.(F) Optical photomicrographs of thin section(PPL) showing the dissolved pore related with the enlarged dissolution of the micro-fractures.wellXC15,3962.66m, T_3x^4.

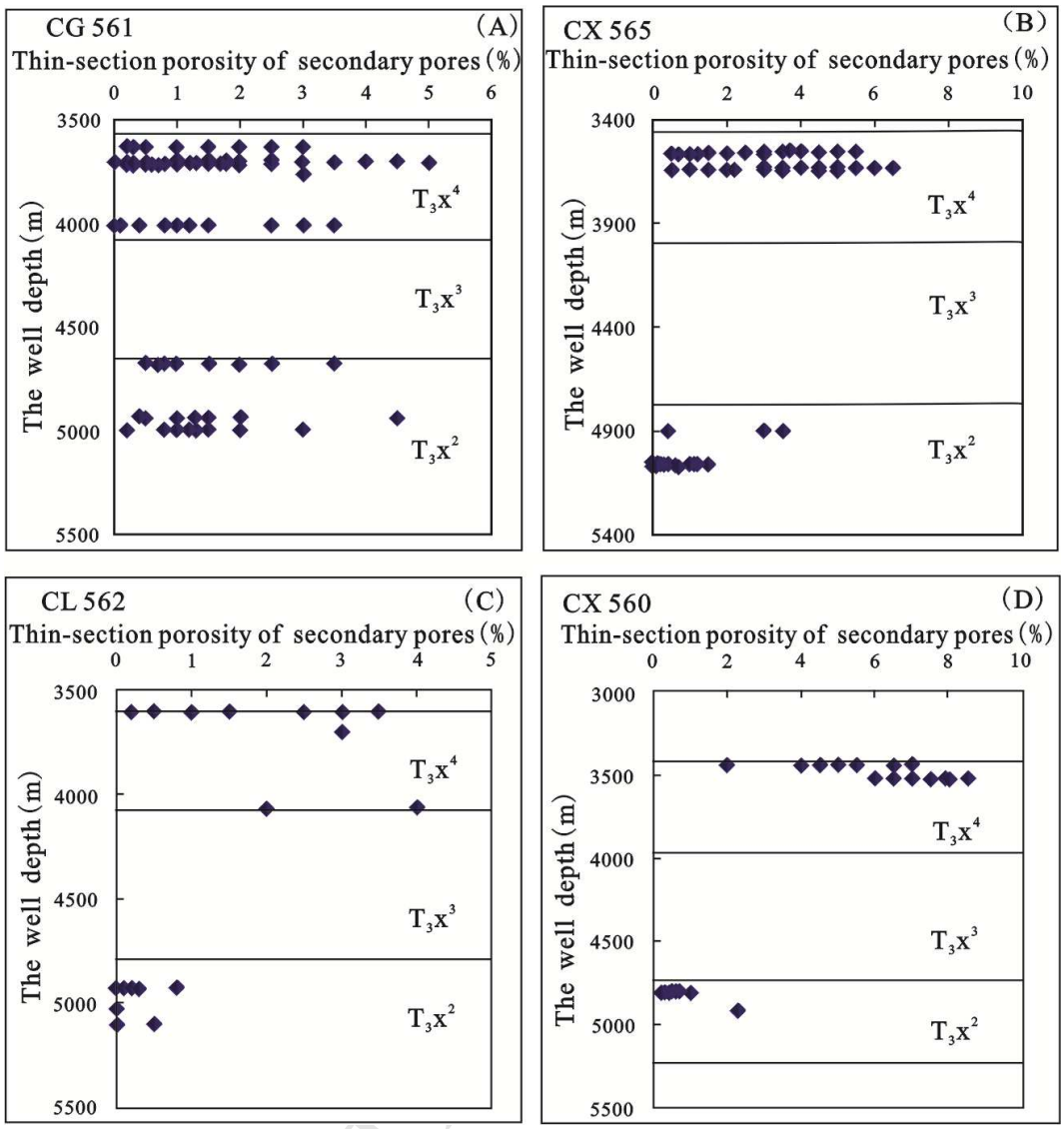

Fig. 16. Distribution characteristic of the secondary pores within the Xujiahe Formation sandstones reservoir of study area (Zhang, 2011). (A) ,(B) ,(C) and (D) show that most of secondary pores usually occurred in the top of the T_3x^4, and some others in the bottom of the T_3x^4 and the middle-upper part of T_3x^2.

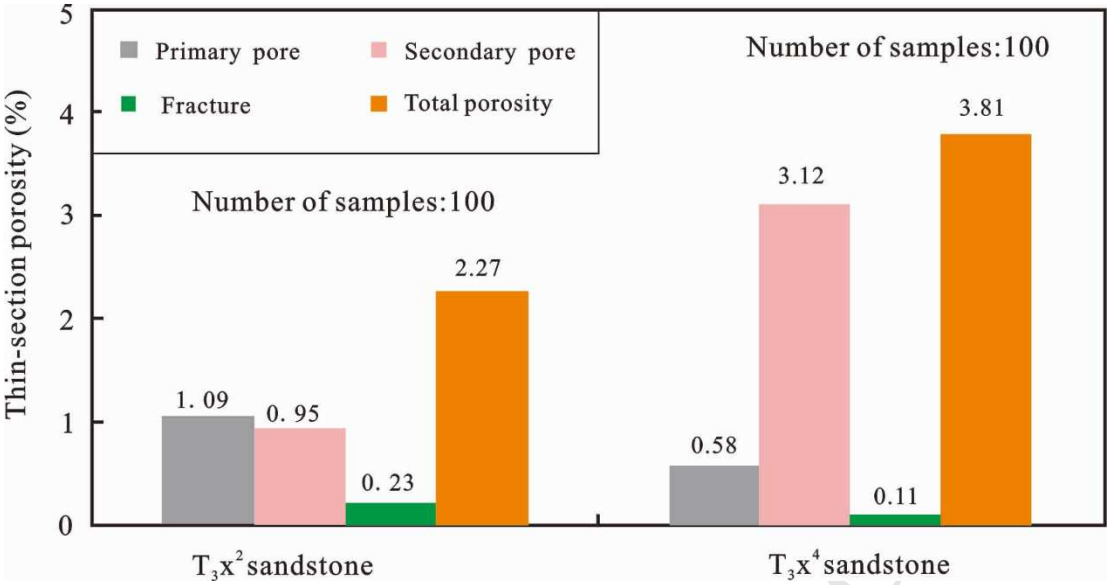

Fig. 17. Thin-section porosity of different types of pore in the T_3x^2 and T_3x^4 sandstone.

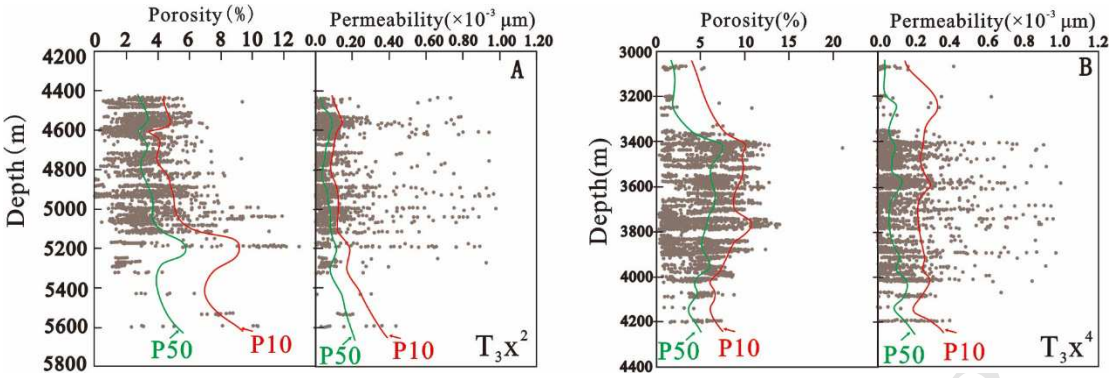

Fig. 18. Core porosity versus depth and core permeability versus depth profiles of the T_3x^2 sandstones (A) and T_3x^4 sandstones (B) in the Xinchang structural belt. Porosity values and permeability values of P10 (10% of reservoir has porosity greater than this value), P50(median) values were calculated for each 0.2-km(0.124-mi)depth interval from starting depth of 4.2km(T_3x^2) and 3.0km(T_3x^4) respectively.

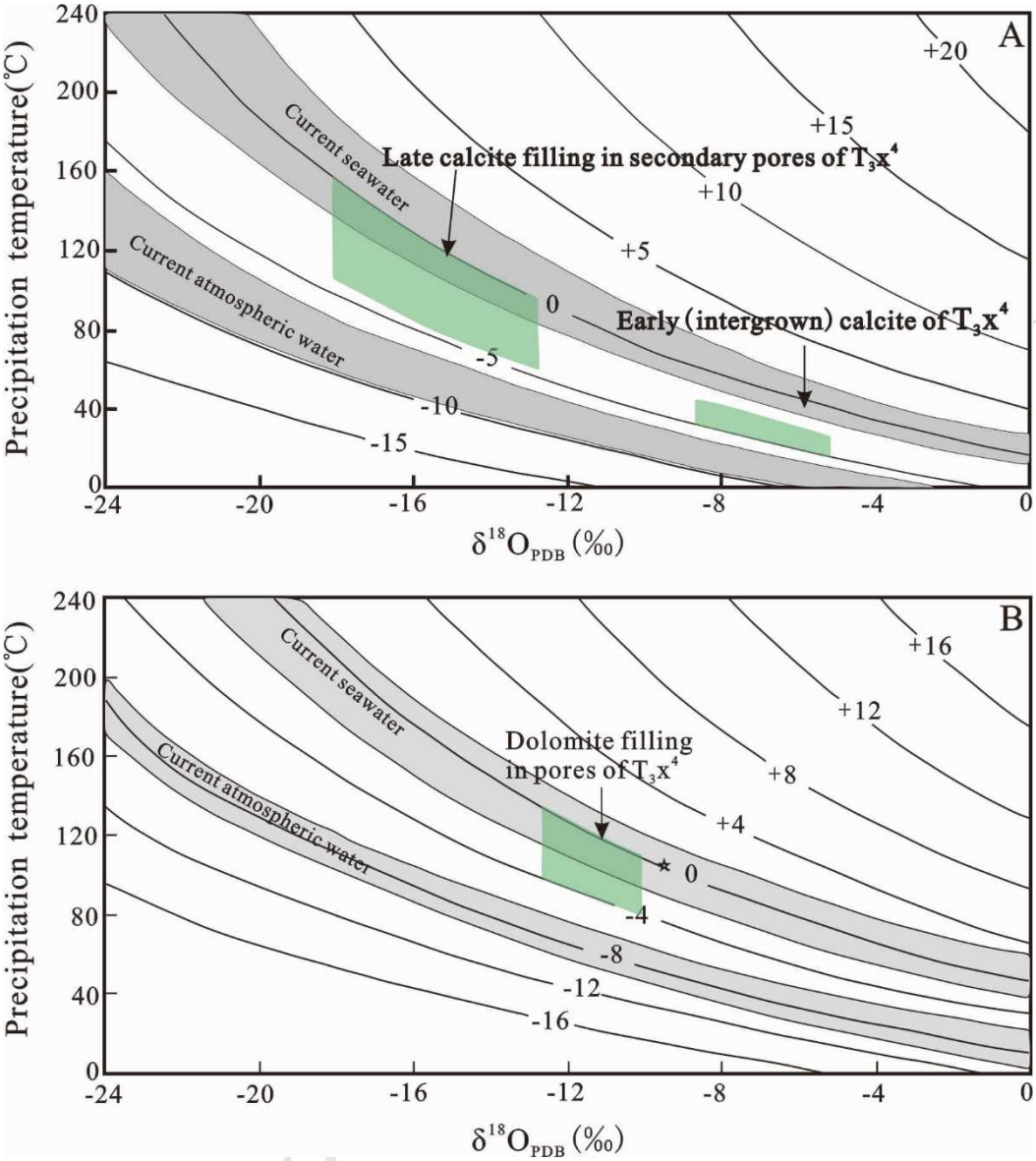

Fig. 19. Cross plot of $\delta^{18}O_{PDB}$ values of the authigenic calcite (A) and dolomite cements(B) within the T_3x^4 sandstones in the Xinchang structural belt in equilibrium with water $\delta^{18}O_{(SMOW)}$ values (-15‰, -10‰, -5‰, 0‰, +5‰, +10‰, +15‰, +20‰) as a function of precipitation temperature (Friedman and O'Neil, 1977). The contours (SMOW) represent oxygen isotopic composition of carbonate balanced fluids. The $\delta^{18}O_{\ water\ (SMOW)}$ values of carbonate balanced fluids within the T_3x^4 sandstones originate from the Liu et al., 2014a,b and Shen et al.,2010.The green shapes were bounded by the authigenic carbonate cements and the δ18O $_{water}$ (SMOW) values of carbonate balanced fluids.

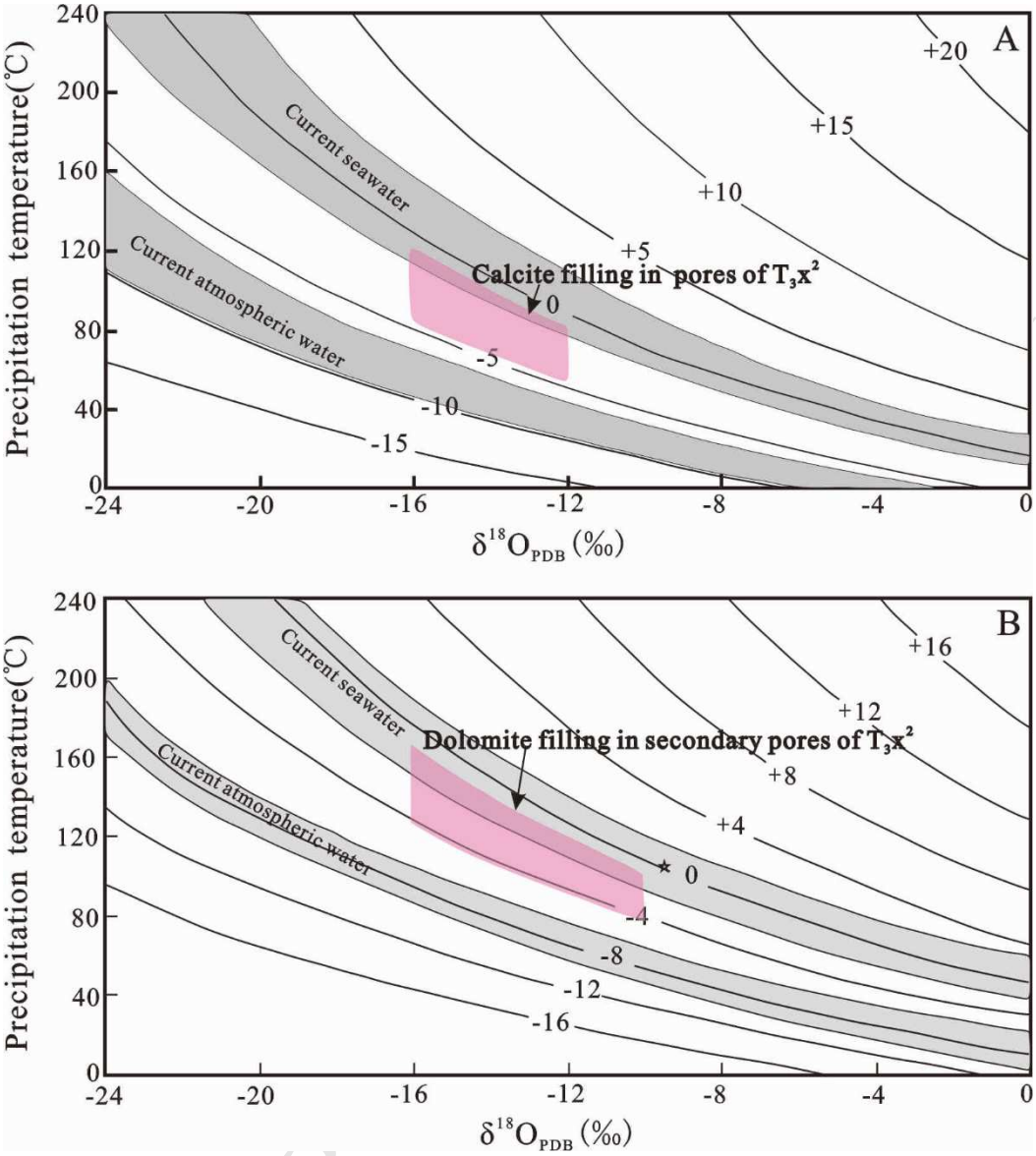

Fig. 20. Cross plot of $\delta^{18}O_{PDB}$ values of the authigenic calcite (A) and dolomite cements(B) within the T_3x^2 sandstones in the Xinchang structural belt in equilibrium with water $\delta^{18}O_{(SMOW)}$ values (-15‰, -10‰, -5‰, 0‰, +5‰, +10‰, +15‰, +20‰) as a function of precipitation temperature (Friedman and O'Neil, 1977). The contours (SMOW) represent oxygen isotopic composition of carbonate balanced fluids. The $\delta^{18}O_{\ water\ (SMOW)}$ values of carbonate balanced fluids within the T_3x^2 sandstones originate from the Liu et al., 2014a,b and Shen et al.,2010. The green shapes were bounded by the authigenic carbonate cements and the δ18O $_{water}$ (SMOW) values of carbonate balanced fluids.

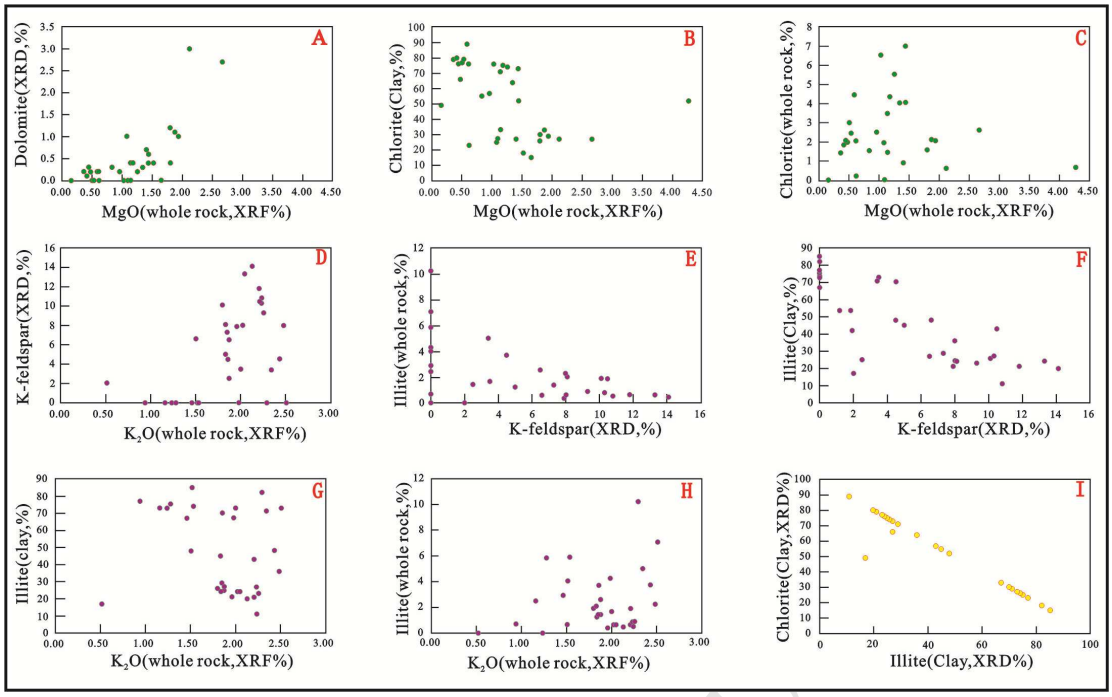

Fig. 21. Scatter diagram between the mineral content and major elements abundances in the in the T_3x^2 sandstones. The mineral content were measured by the XRD (data from the table 1 and Fig.12).The major elements abundances were measured by the XRF (data from table 6 and Fig.12).

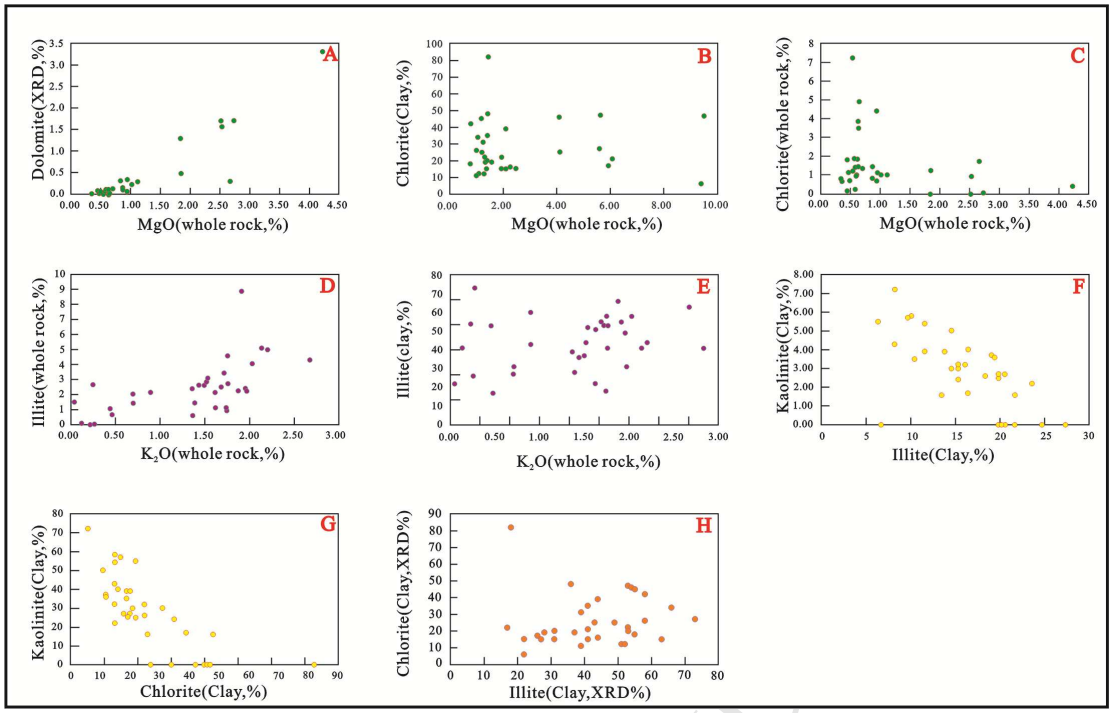

Fig. 22. Scatter diagram between the mineral content and major elements abundances in the in the T_3x^4 sandstones. The mineral content were measured by the XRD (data from the table 2 and Fig.13).The major elements abundances were measured by the XRF (data from table 7 and Fig.13).

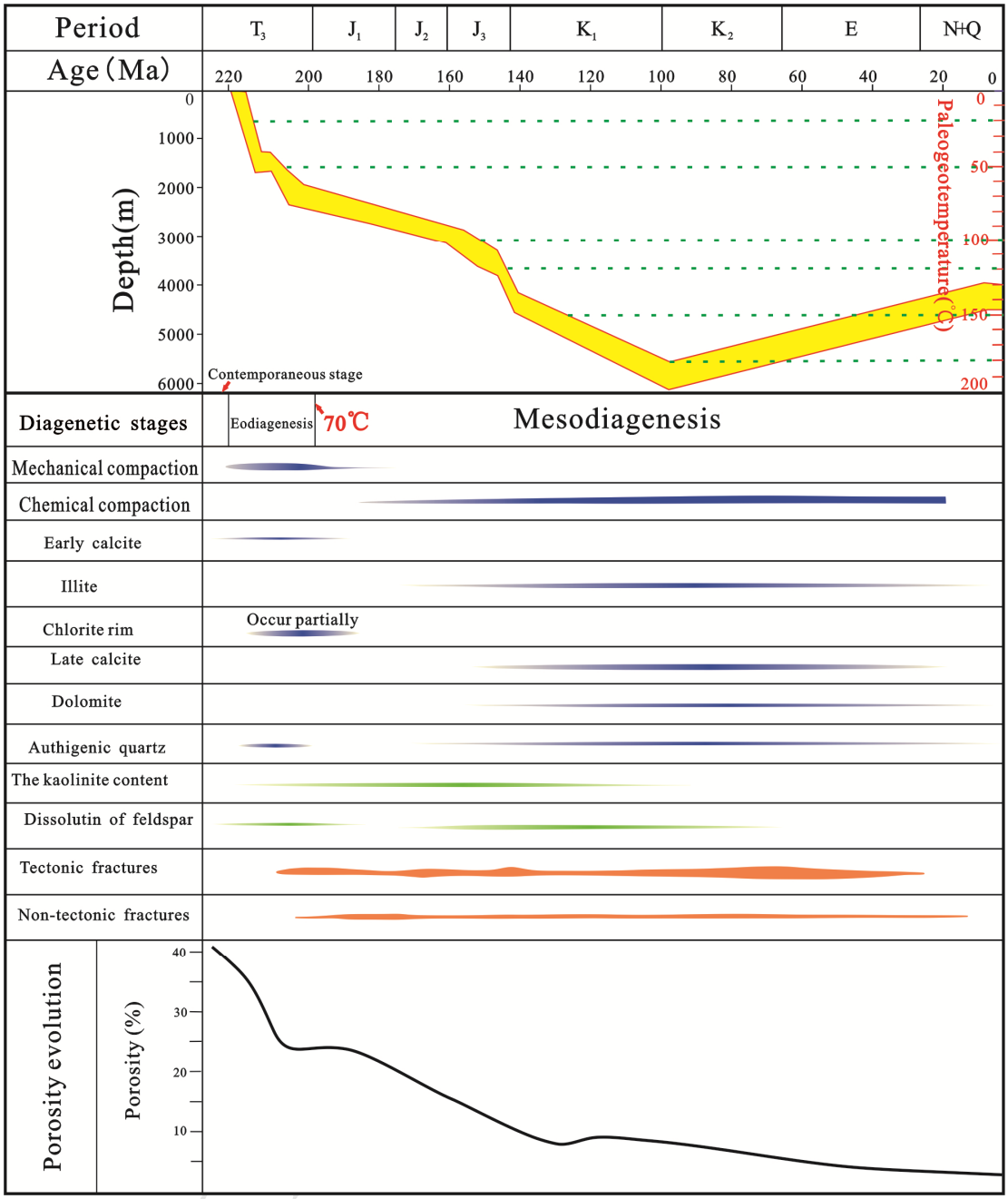

Fig. 23. Burial, thermal, diagenetic history and evolution of porosity in the T_3x^2 sandstone. The paragenetic sequence showing the relative timing and strength of the diagenesis based on petrographic relationships, diagenetic characters and fluid inclusion. Burial and thermal history, porosity evolution and the characteristics of fractures were presented on the basis of previous studies (Zhang,2005; Zeng,2010; Luo ,2015).

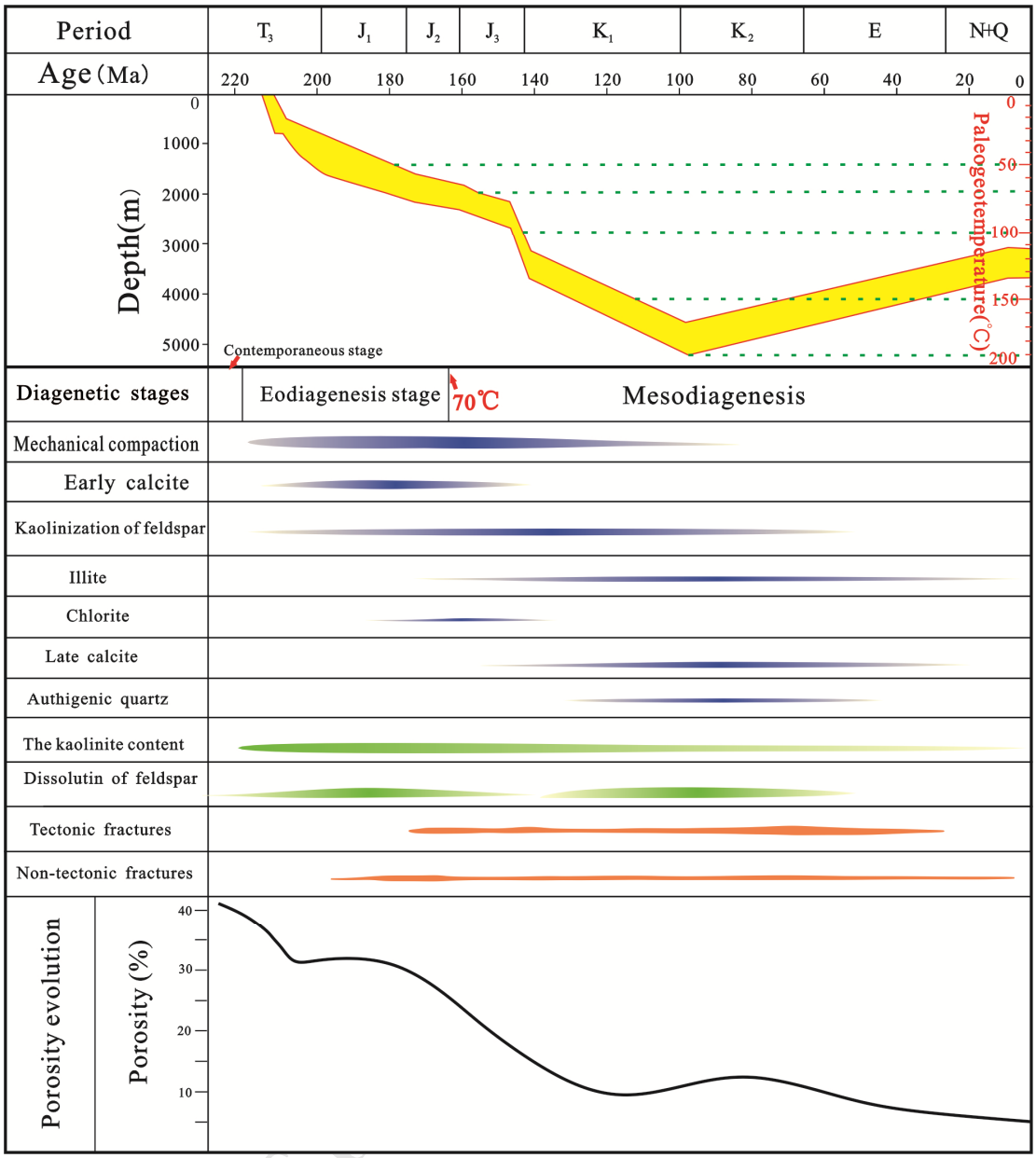

Fig. 24. Burial, thermal, diagenetic history and evolution of porosity in the T_3x^4 sandstone. The paragenetic sequence showing the relative timing and strength of the diagenetic alterations relying on petrographic relationships, diagenetic characters and fluid inclusion. Burial and thermal history, porosity evolution and the characteristics of fractures were presented on the basis of previous studies (Zhang,2005; Zeng,2010; Luo ,2015).

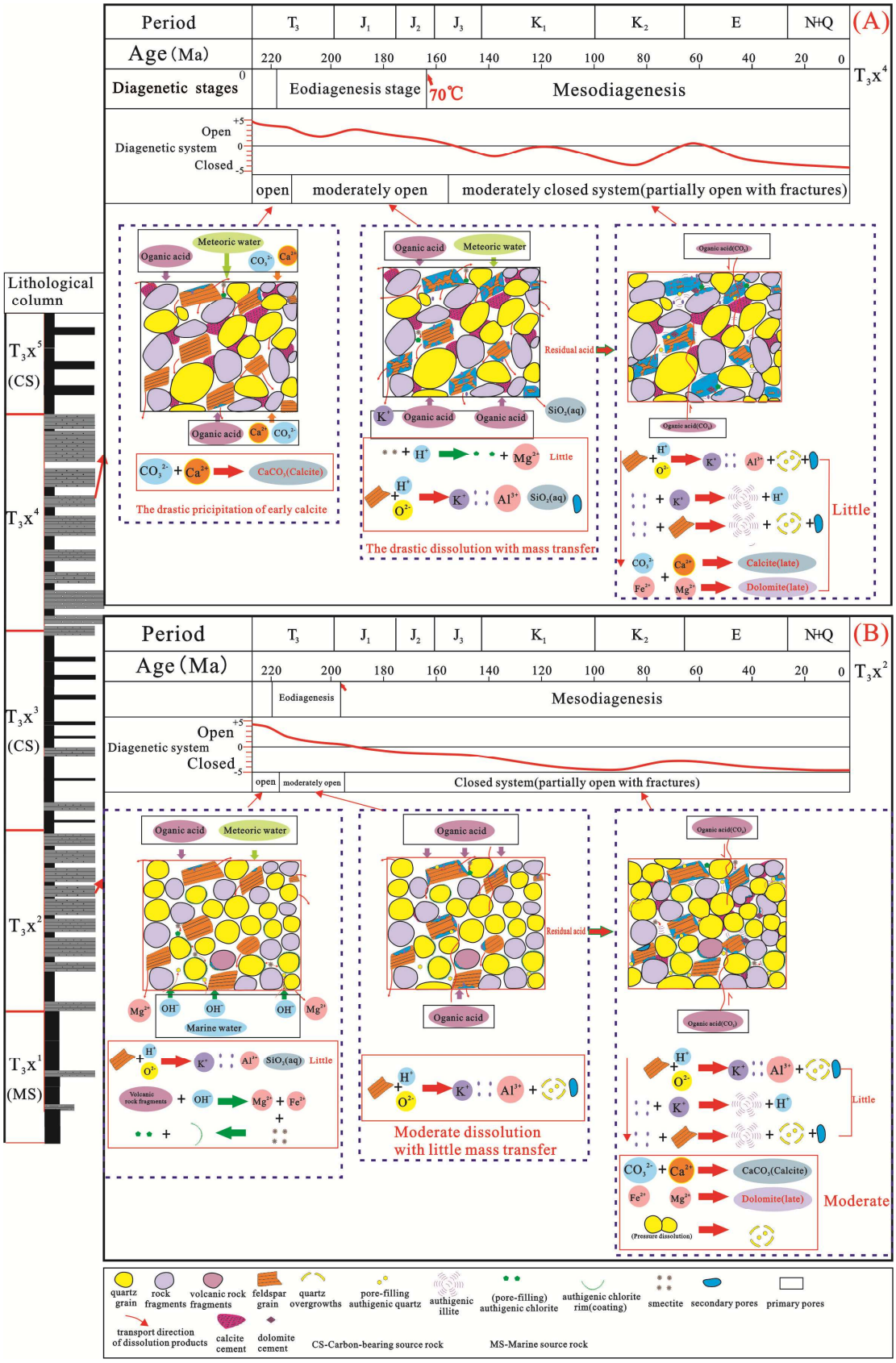

Fig. 25. A conceptual model summarizing the diagenetic system of the T_3x^4 sandstone (A) and T_3x^2 sandstone (B). This model indicates the origin, diagenetic relationship,

controlling factors and evolution of diagenetic system.

1.Tight deltaic sandstones have undergone obvious changes of geochemical composition

2. Dissolution was main source of pore space in the T_3x^2 and T_3x4 sandstones

3. The diagenetic systems were open at near-surface, eodiagenesis and early mesodiagenesis

4.Diagenetic systems were nearly closed in middle-late mesodiagenesis except for fractures zone.

5. Open system produced secondary pores and provided kaolinite and K^+ for illitization.